

Bio-inspired Legged Locomotion

.....

Chapter 5

Torque control in legged locomotion

Juanjuan Zhang^{1,2}, Chien Chern Cheah², and Steven H. Collins^{1,3}

Many torque control approaches have been proposed for robotic devices used in legged locomotion, but few comparisons have been performed across controllers in the same system. In this study, we compared the torque-tracking performance of nine control strategies, including variations on classical feedback control, model-based control, adaptive control and iterative learning. To account for interactions between patterns in desired torque and tracking performance, we tested each in combination with four high-level controllers that determined desired torque based on time, joint angle, a neuromuscular model, or electromyographic measurements. Controllers were implemented on an ankle exoskeleton with series elastic actuation driven by an off-board motor through a uni-directional Bowden cable. The exoskeleton was worn by one human subject walking on a treadmill at $1.25 \text{ m}\cdot\text{s}^{-1}$ for one hundred steady-state steps under each condition. We found that the combination of proportional control, damping injection and iterative learning resulted in substantially lower root-mean-squared error than other torque control approaches for all high-level controllers. With this low level torque controller, RMS errors can be as low as 1.3% of peak torque for real-time tracking, and 0.2% for the average stride. Model-free, integration-free feedback control seems to be well suited to the uncertain, changing dynamics of the human-robot system, while iterative learning is advantageous in the cyclic task of walking.

5.1 Introduction

Robotic legged locomotion, including walking robots and powered lower-limb exoskeletons and prostheses, has been an area of active research for decades [1–3]. Most early walking related robots used kinematic trajectory control, an approach that persists today [4–7]. In case of exoskeletons and prostheses, however, position control strategies tend to result in less safe and less comfortable human-robot interactions since they can cause large forces to develop when human and robot motions differ [8, 9]. Position-controlled exoskeletons have also been shown to be less effective in rehabilitation compared to traditional human-based therapies [10] for similar reasons.

Increasingly, the control of exoskeletons and prostheses has shifted from kinematic methods to strategies that respond more fluidly to actions of the user. One reason for this shift is the concern for human safety and comfort. Another driver is our improved understanding of the natural dynamics of human motion [11–15], which suggests a more dynamic approach to human-robot interactions than afforded by kinematic control.

One method for improved interaction between humans and robots is impedance manipulation [16], in which the reaction of a robot to external forces is regulated rather than the resulting position trajectory [17]. Whereas position control strategies typically impose high impedance to improve trajectory tracking performance, this method allows lower impedance at the robot interface and a greater influence of human actions on the resulting motions.

¹Dept. Mechanical Engineering, Carnegie Mellon University, USA.

²School of Electric and Electronic Engineering, Nanyang Technological University, Singapore.

³Robotics Institute, Carnegie Mellon University, USA.

Direct control of interaction forces or torques can also be used to reduce human-robot interface impedance [9, 18]. Torque control provides a simple means of manipulating the flow of energy from the exoskeleton to the human, which can be useful in biomechanics studies [19–23]. Torque control can also be used to exploit passive dynamics or render virtual systems with alternate dynamics in humanoid robots [24], active prostheses [25–27], and exoskeletons [28–31]. In exoskeletons and prostheses, the quality of torque control is a limiting factor in precision of the applied intervention and can be the limiting factor in human-robot system performance.

Series elastic actuation, in which compliance is placed between a motor and its end-effector, can improve torque control in devices. This is especially important when human-robot interaction is involved, in which case there often exists unknown, changing human-exoskeleton interaction dynamics. Elasticity in the actuator transmission decouples motor inertia from the structure of the exoskeleton or prosthesis [32], which physically reduces interface impedance and results in smaller torques when human and robot motions unexpectedly diverge. Series elastic actuation can thereby provide improved human safety [33] and improve torque tracking performance in the face of complex, dynamic user movements [34]. Unlike direct-drive actuators, torque output in a series elastic actuator is usually not directly related to motor torque, but instead to the position of the motor relative to the joint. Motor position is therefore better correlated to load torque, especially in the presence of transmission friction. For these reasons, series elastic actuators with a motor drive running in velocity mode typically have lower actuation impedance and smoother torque tracking with lower error [35, 36].

Bowden cable transmissions are often used in exoskeletons and prostheses to further reduce physical impedance through drive relocation. Bowden cables allow motor and gearbox elements to be placed in more desirable locations than the joint they actuate, resulting in reduced device inertia. Motors can be moved proximally on the limb or body [13, 37–39] or off the body altogether [27, 31, 40]. Bowden cables are flexible, producing little interference with joint motions [41], but have complex stick-slip transmission dynamics that pose additional torque control challenges [37].

Unidirectional Bowden cables can completely isolate the human from motor inertia when desired. The capacity to become transparent, or produce zero impedance, is desirable in exoskeletons, as it is frequently useful to apply precisely zero torque to the human [19, 42–44]. Uni-directional Bowden cables can be kept slack, preventing any torque from being transmitted regardless of human dynamics [23, 31, 45]. However, allowing the transmission to become slack introduces complex dynamics and uncertainty during re-engagement, as in other systems with intermittent contact, which can make torque control more difficult.

The human ankle produces more than half of the mechanical work of the lower limbs during walking [46] and has been a frequent target for exoskeleton and prosthesis assistance [47] and humanoid robot control [48]. In fact, ankle joint assistance has led to the first systems that reduce the energy cost of walking for humans [22], including one device that does so passively [49]. Improved torque control at ankle joints of robotic legged locomotion systems would provide immediate benefits for such systems, and could also be beneficial at knee and hip joints.

Torque control is typically implemented at a low level in walking-related robot control hierarchies, with higher level controllers determining behaviors and commanding desired torques. In such schemes, desired torque is not a control objective selected in advance, but rather a mid-level signal, often with complex dynamics that reflect interactions with the human user. In this chapter, we will refer to the class of control elements that generate desired torque as *high-level controllers*, and to the elements that enforce desired torque, the torque controllers that are the primary focus of this study, as *low-level controllers*. Since the dynamics of the desired torque signal depend on the high-level control type, we expect interactions with low-level controllers that will affect torque tracking performance.

Many potential low-level control elements have been proposed for tracking torque and position in walking related robots and series elastic actuators. Prominent categories of torque control include classical feedback, model-based control, adaptive control and iterative learning.

Classical proportional-integral-derivative (PID) feedback control, and simple variations thereon, have been widely employed in exoskeletons due to their simplicity and ease of tuning. Integral control elements are used to reduce steady state errors in series elastic actuators with consistent dynamics and low impedance [30, 35, 36, 44, 50–52]. Integration-free proportional-derivative (PD) control is often used in high-impedance exoskeletons [53–55] and in series elastic actuators with more modeling uncertainties [41, 42]. In cases where the derivative of the error signal is noisy, damping injection, or negative feedback on a less noisy velocity in the system, can be used instead to provide similar stabilizing effects [56, 57]. Gain scheduling, in which control gain values change according to system states, is sometimes used in the control of robots that interact with humans for improved safety or intervention efficiency [58–60].

Model-based control elements are often used in robots to improve torque-tracking performance. Approaches typically include feed-forward terms that use inverted plant dynamics to shape impedance or torque [5, 17, 35, 44, 52, 61]. This approach works best with an accurate model of the system.

Adaptive control has also often been used in systems with human-robot interaction [62]. One example of adaptive control that has been applied to human-robot interaction is passivity-based control. These controllers manipulate the energy balance of the system using a system model and adaptive control elements, and can improve tracking performance with provable closed-loop stability [63]. Passivity-based control has been proposed for series elastic actuators [64] and used during human-robot interactions [62].

Variations on iterative learning derived from industrial robots have also been applied to robotic legged locomotion [44, 65]. This approach improves tracking performance by exploiting the cyclic nature of gait; tracking errors from past walking steps are used to predict errors in the ensuing step, and feed-forward corrections are applied. Since corrections are based on an accumulation of past errors, this approach bears some resemblance to classical integral control, in which errors in previous steps are used to improve performance during the present step.

High-level controllers intended to assist human walking include schemes that command desired torque based on time, joint angle, neuromuscular models, and electromyographic measurements. Perhaps the simplest way to generate desired torques is as a function of time, which can be used to regulate the relative timing of robot actions as well as human actions in cases of exoskeletons and prostheses [22, 23, 66]. Another common method is to imitate observed relationships between human joint angles and joint torques [25, 67, 68], which can be especially useful in regulating net joint work [41]. Virtual neuromuscular systems with complex internal dynamics have also been used to generate desired joint torques in assistive devices [69–76]. This method has demonstrated benefits in the control of adaptive prosthetic limbs [77]. Direct neuromuscular interfaces, such as through electromyographic measurement of muscle activity, promise more intuitive control of exoskeletons by users [28, 47, 61, 78–80]. Each of these high-level control approaches may be advantageous in some assistance paradigm, and each results in desired torque signals with different dynamics.

Many approaches to torque control in robotic legged locomotion have been established, but a more complete comparison would be helpful when designing controllers for new systems. The classical feedback, model-based, adaptive and iterative learning control approaches reviewed in this section all have strengths for human-robot interaction. Several of these controllers have been tested in lower-limb exoskeletons and have shown good performance [30, 40, 43, 44, 81, 82]. Comparisons across studies are made difficult, however, due to differences in protocol, performance metrics, hardware, and high-level controllers. Some results are reported for benchtop tests [83–85], which may provide more positive results than during complex interactions with humans. Some results are not reported quantitatively [81], which makes comparisons difficult. In some cases a small number of controllers have been tested on the same hardware [44], but in most cases torque tracking results are provided for a single controller working with a single system. This makes comparisons across studies difficult, since some portion of the differences in performance may be due to differences in the capability of the hardware used. Similarly, comparisons have been performed with different high-level controllers, which could interact with low-level controllers and contribute to differences in performance across studies. Studies comparing a wide range of torque controllers in human-interaction protocols with quantitative performance metrics, consistent hardware setups and a variety of high-level controllers would help establish guidelines for selecting and tuning controllers for new robotic legged locomotion systems.

The aim of this chapter is to compare the tracking performance of prominent torque control methods, with multiple high-level desired torque conditions, in a single robotic legged locomotion platform during walking. Promising methods using classical feedback, model-based, adaptive and iterative learning control elements were used. Although it was impractical to test all possible control strategies, the chosen controllers span the set of candidate methods and provide a more comprehensive test than previously available. A diverse sample of high-level controllers were used to test for interactions with low-level control dynamics and provide insights into the generality of tracking results. A single exoskeleton system was used, experimentally controlling for hardware capabilities. Tests were conducted while a human wore the exoskeleton and walked on a treadmill, making results relevant to conditions with complex interactions between the robot, a human user, and the environment. We anticipate these results to help guide the selection and tuning of torque control elements in various robotic legged locomotion systems.

5.2 System Overview

5.2.1 System Modeling

A diagram of a typical one degree-of-freedom lower-limb robot driven by a series elastic actuator through a cable with a geared motor is shown in Fig. 5.1. Based on this structure, we used the following simplified models of system

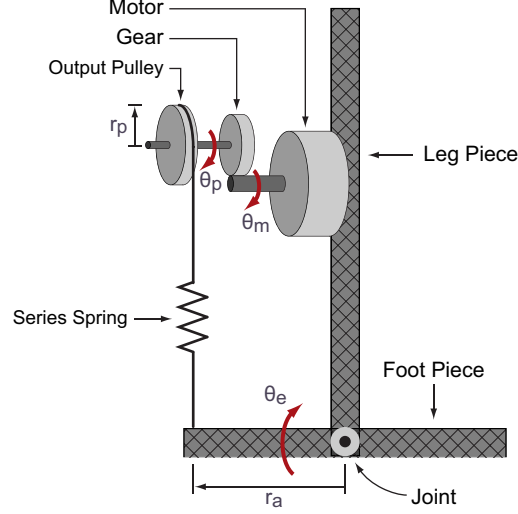


Figure 5.1: A schematic diagram of a one degree-of-freedom, cable-driven, robotic legged locomotion system with a series elastic actuator. This diagram uses an ankle device as an example. θ_m and θ_p are motor position and pulley position after gearing respectively. θ_e is the device joint angle. R is the effective aspect ratio between motor output pulley radius r_p and device joint velocity lever arm r_a defined as $R = \frac{r_a}{r_p}$.

components to aid in our understanding of the system, make reasonable choices for model-free control elements, and design model-based control elements.

◇ Motor Dynamics

Assuming armature inductance dynamics occur at a substantially higher frequency than rotor dynamics, and therefore have negligible effects, the dynamics of the motor can be written as

$$\begin{cases} K_a \cdot i_a(t) = I_e \cdot N \cdot \ddot{\theta}_p(t) + f_e \cdot N \cdot \dot{\theta}_p(t) + \frac{1}{N} \cdot \tau_o(t), \\ V_a(t) = R_a \cdot i_a(t) + K_b \cdot N \cdot \dot{\theta}_p(t) \end{cases}, \quad (5.1)$$

in which K_a is the motor-torque constant, i_a is the armature current, I_e is the effective moment of inertia of the motor and gear referred to the motor shaft, $N = \dot{\theta}_m / \dot{\theta}_p$ is the gear ratio, θ_m is the angular position of the motor shaft, θ_p is the angular position of the gear output shaft, f_e is the effective viscous friction coefficient of the combined motor and gear referred to the motor shaft, τ_o is output torque at the gear output pulley, V_a is the armature voltage, R_a is the armature resistance, and K_b is the motor voltage constant.

◇ Transmission Model

The pulley transmits load to the cable as

$$\tau_o = F \cdot r_p \quad (5.2)$$

in which r_p is the radius of the pulley attached to the gear output and F is the tension in the cable on the motor side. Making the simplifying assumption that there is no friction in the transmission, the torque at the device side is

$$\tau = F \cdot r_a, \quad (5.3)$$

in which r_a is the lever arm at the ankle joint. We further assume that the angular excursion of the ankle joint is small, and that the lever arm is therefore approximately constant.

◇ Force-Position Relationship

Making the simplifying assumption that the cable has either spring-like compliance or negligible compliance compared to the series spring, we have

$$F = K_c \cdot (r_p \cdot \theta_p - r_a \cdot \theta_e) \quad (5.4)$$

in which K_c is the total effective stiffness of the cable transmission and series spring and θ_p and θ_e are the pulley and device joint angles relative to a neutral position at which the cable begins to go slack.

◇ Torque-Angle Relationship

Defining the gear ratio of the transmission, R , as

$$R = \frac{r_a}{r_p} \quad (5.5)$$

the torque applied by the device can be written as

$$\begin{aligned} \tau &= F \cdot r_a \\ &= r_p \cdot r_a \cdot K_c \left[\theta_p - \frac{r_a}{r_p} \theta_e \right] \\ &= K_t (\theta_p - \theta_e R) \end{aligned} \quad (5.6)$$

with transmission stiffness, K_t , defined as

$$K_t = r_p \cdot r_a \cdot K_c \quad (5.7)$$

relating torque at the device to the angles of the motor output pulley and device joint.

◇ Device Joint Dynamics

Applying law of balance of angular momentum to the device joint, we have

$$\tau - \tau_h - B_e \cdot \dot{\theta}_e = I_e \cdot \ddot{\theta}_e \quad (5.8)$$

where τ_h is the torque applied to the robot by the environment, which is mostly human body in case of exoskeletons, B_e is the device joint damping coefficient, and I_e is the moment of inertia of the device.

◇ Motor Velocity Control Dynamics

Motors are often operated in velocity control mode in series elastic actuators, which tends to result in lower actuation impedance and better torque tracking [35, 36]. Without access to the proprietary controller used by the commercialized motor drivers, the precise relationship between desired motor velocity, $\dot{\theta}_{m,des}$, and input voltage to the motor, V_a , is unknown. However, from Eq. (5.1), we can derive the relationship between input voltage and actual motor velocity as

$$\begin{aligned} V_a &= \frac{R_a I_e N}{K_a} \ddot{\theta}_p + \left(\frac{R_a f_e N}{K_a} + K_b N \right) \dot{\theta}_p + \frac{R_a}{K_a} \tau_o \\ &= \frac{R_a I_e}{K_a} \ddot{\theta}_m + \left(\frac{R_a f_e}{K_a} + K_b \right) \dot{\theta}_m + \frac{R_a}{K_a} \tau_o \end{aligned} \quad (5.9)$$

When the angular acceleration is zero, this reduces to

$$V_a = \left(\frac{R_a f_e}{K_a} + K_b \right) \dot{\theta}_m + \frac{R_a}{K_a} \tau_o. \quad (5.10)$$

At moderate torques and speeds, the contribution of armature resistance to voltage drop is small at moderate speeds. Neglecting this term, we have

$$V_a = \left(\frac{R_a f_e}{K_a} + K_b \right) \dot{\theta}_m, \quad (5.11)$$

and input voltage and motor velocity are linearly related at low torque and high speed.

5.2.2 Potential Control Issues

While the dynamic models described by Eq. (5.1)-(5.11) capture the basic properties of the system, they do not address its full complexity. There are additional uncertain or changing dynamics that are difficult to model, which contribute to most of the challenges of the control problem we are addressing. These additional complexities are described below.

◇ Bowden Cable Nonlinearities and Stiction

Bowden cables are often used as a part of the transmission in robotic legged locomotion systems. For simplicity, we modeled the Bowden cable as a frictionless linear spring, but its stiffness is actually nonlinear and there are substantial frictional effects. The cable is stiffening, exhibiting greater local stiffness at high loads. This can be seen in the torque versus ankle angle curves generated by fixing the motor and passively flexing the device joint during walking (Fig. 5.2). The cable warms over the course of a many strides, which decreases its overall stiffness. It exhibits creep, which increases the slack length. If the cable is allowed to go slack, the state corresponding to re-engagement is uncertain. There is substantial friction in the cable, including dissipation with characteristics of Coloumb friction, viscous damping, and stiction, some of which are visible in Fig. 5.2. The cable heats over the course of many strides, which increases overall friction. Stiction leads to sudden changes in cable force, and propagation of the slipping point along the length of the cable makes these changes unpredictable. These transmission properties are complex, nonlinear and time varying.

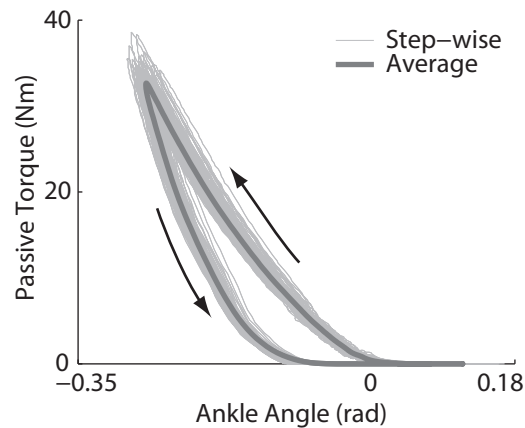


Figure 5.2: Torque versus exoskeleton ankle joint angle relationship with motor position fixed and the ankle joint being passively flexed for one hundred strides.

◇ Human-Robot Interaction and Human Adaptation

In the case of exoskeletons and prostheses, the robot device works together with the human body. The device often contacts the soft tissues and muscles of the human body, often using flexible straps. This interface is complex and nonlinear, with low overall impedance. For example, muscle activity beneath the straps can substantially affect stiffness and damping at the interface. Straps may also shift on the limb, altering lever arms and engaging different tissues. Human kinematics, kinetics and underlying neural and muscular activity also vary in time and across steps. This can be seen in the variations in ankle joint angle curves over many steps, even when the motor position is fixed (Fig. 5.3).

◇ Delays Caused by Communication and Motor Velocity Tracking

Delays in generating desired motor position also pose a control challenge. A portion of these delays can come from communication between subsystems. For example, in the hardware used in this study there was a 6 ms closed-loop communication delay. Another effective delay comes from accelerating the motor rotor. For the hardware used in this study the motor velocity rise time was about 7 ms. These delays cause feedback controllers to become unstable as gains are increased, limiting closed-loop performance.

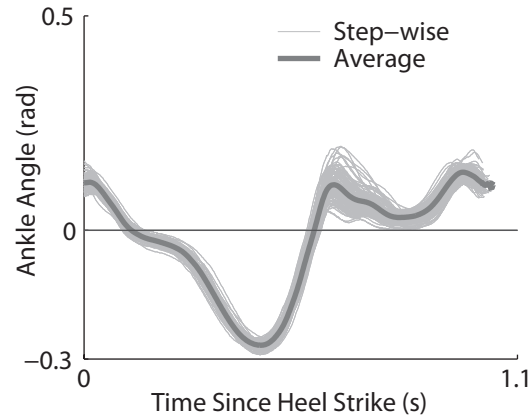


Figure 5.3: Variability in exoskeleton ankle joint angle trajectory during one hundred strides of walking with the motor position fixed and the ankle exoskeleton passively flexing.

An effective low-level torque controller must accommodate these complex, nonlinear, time-varying system features. As discussed in the Introduction section, various control methods have been employed in addressing this issue, which include model-free and model-based controllers that were used as feedback or feed-forward elements. These methods span the range of classical proportional-integral-derivative control, passivity-based control, model-based feed-forward compensation and iterative learning compensation. The relative performance of these control approaches will be investigated in this chapter with an experimental case study in an ankle exoskeleton testbed, which will be detailed in the next section.

5.3 A Case Study with an Ankle Exoskeleton

To investigate the relative performance of various control methods in torque tracking for robotic legged locomotion, a case study was conducted. We compared torque tracking performance for nine common torque control methods that used combinations of classical feedback control, model-based control, adaptive control and iterative learning. These included examples of model-free and model-based feedback and feedforward control. Each low-level torque controller was tested with four high-level walking controllers that set desired torque based on time, ankle angle, a neuromuscular model, or electromyographic measurements. All controllers were implemented on a tethered ankle-foot exoskeleton with series-elastic actuation driven by a uni-directional Bowden cable, and each was tuned to minimize error. The exoskeleton was then worn by one subject who walked on a treadmill for one hundred strides at steady state under each condition, and the root mean squared errors between desired and measured torque were calculated for each stride and for the averaged stride.

5.3.1 Exoskeleton system

We tested on a tethered ankle exoskeleton that was comprised of an off-board real-time control module and geared electric motor, a uni-directional Bowden cable transmission with a series spring, and an exoskeleton frame that interfaced with the human foot and shank (Fig. 5.4). This system is described in detail in Witte et al. (2015) [31], and a summary is provided below.

We used a dedicated real-time control system (ACE1103, dSPACE Inc.) to sample sensors at 5000 Hz, filter sensor data at 200 Hz, and generate desired motor velocity commands at 500 Hz. The motor unit was composed of a low-inertia, 1.6 kW AC servo motor and a 5:1 planetary gear, with input voltage regulated by a motor driver running in velocity control mode (BSM90N-175AD, GBSM90-MRP120-5 and MFE460A010B, Baldor Electric Co.). A digital optical encoder (E4, US Digital Corp.) measured motor position. As an indication of motor module performance, the 100% rise time to peak motor velocity was 0.013 s.

A flexible uni-directional Bowden cable transmitted forces from the motor to the exoskeleton frame while minimally restricting leg motions. The cable was composed of a coiled-steel outer conduit (415310-00, Lexco Cable Mfg.)

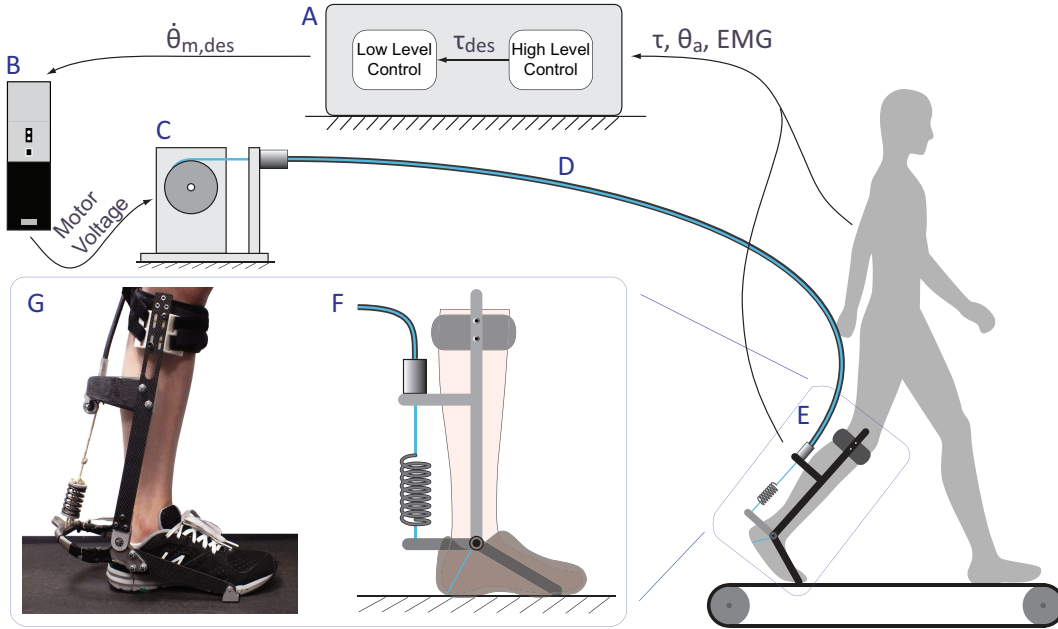


Figure 5.4: Experimental Testbed: A) A real-time controller reads sensory information, computes desired torques using a high-level controller, computes desired motor velocity using a low level controller, and outputs desired motor velocity to the motor drive. B) A dedicated motor drive. C) An off-board geared motor and pulley. D) A Bowden cable transmission. E) A lightweight instrumented ankle exoskeleton. F) A enlarged schematic of the exoskeleton. G) A photograph of the exoskeleton.

and a 0.003 m diameter Vectran[®] inner rope, and was 2 m in length. A series spring (DWC-148M-12, Diamond Wire Spring Co.) with an effective stiffness of $190 \text{ N}\cdot\text{m}\cdot\text{rad}^{-1}$ (in terms of ankle rotation) was attached at the end of the rope to provide increased compliance.

The exoskeleton frame applied forces on the front of the human shank below the knee, beneath the heel, and on the ground beneath the toe, so as to generate an ankle plantarflexion torque in proportion to transmission force. Torque was measured using strain gauges (MMF003129, Micro-Measurements) applied in a full Wheatstone bridge on the heel lever, with 1000 Hz signal conditioning (CSG110, Futek Inc.). Joint angle was measured using a digital optical encoder (E5, US Digital Corp.). For one of the high-level controllers, we measured gastrocnemius muscle activity using a wired electromyography system (Bagnoli 4 EMG System, Delsys Inc.).

The high-level and low-level controllers, motor, transmission, exoskeleton frame and human interacted as shown in Fig. 5.5. The high-level controller used time, t , device joint angle, θ_e , or human electromyography, EMG, to determine desired torque. The low-level controller regulated torque, using desired torque, τ_{des} , measured torque, τ , motor angle, θ_m , and/or device angle to command desired motor velocity, $\dot{\theta}_{m,des}$. A hardware motor driver regulated motor velocity. Motor rotations were transmitted through a cable to one end of a series spring. Together with device rotation, this determined spring deflection, which in turn generated device torque. Exoskeleton movements resulted from the balance of torques from the series spring and from the human leg.

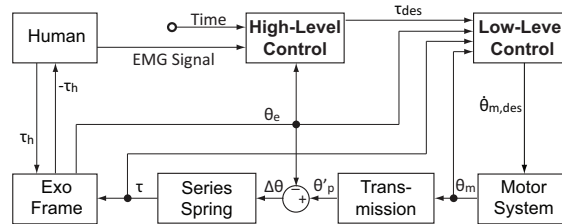


Figure 5.5: Flowchart of the control system. High Level Control and Low Level Control are the two blocks to be varied in this study.

5.3.2 Low-Level Torque Controllers

We tested torque tracking performance with nine prominent low-level torque control methods. Low-level controllers were selected based on prominence in the literature, expected performance based on system modeling, and the results of pilot testing. They included model-free and model-based feedback and feedforward elements. Desired torque was set with each of four high-level exoskeleton control strategies, chosen based on prominence in the literature. High-level controllers set desired torque based on time, joint angle, a neuromuscular model or electromyography.

Motor Velocity Control

All torque controllers investigated in this study included motor velocity control performed by a dedicated hardware motor controller. Series elastic actuators with a drive running in velocity mode typically have lower actuation impedance and smoother torque tracking with lower error [35, 36] than when torque is commanded to the drive. With series elastic actuation, controlling motor velocity is similar to controlling the rate of change of applied torque, since torque is approximated by the product of series stiffness and the difference between motor angle and exoskeleton joint angle (Eq. 5.6). Desired motor velocity was calculated as:

$$\begin{aligned}\dot{\theta}_{m,des} &= \frac{1}{T} \cdot \Delta\theta_{m,des} \\ &= \frac{N}{T} \cdot \Delta\theta_{p,des}\end{aligned}\quad (5.12)$$

where $\dot{\theta}_{m,des}$ is commanded motor velocity, T is a gain related to rise time, $\Delta\theta_{m,des}$ is desired change in motor position, N is the motor gear ratio, and $\Delta\theta_{p,des}$ is desired change in pulley position, determined by one of the low-level torque controllers described below. The value of T was tuned so as to minimize motor position rise time without causing oscillations during torque tracking.

Model-Free Feedback Control

The first group of torque controllers used model-free feedback control, comprising variations on classical proportional-integral-derivative control. Gains were tuned systematically using model-free procedures. Following tuning and pilot testing, four low-level controllers were experimentally compared, $L1-L4$.

$L1$: Proportional Control with Damping Injection (PD*)

This controller was analogous to classical proportional-derivative control of torque, with damping injection [56, 57] on motor velocity taking the place of the derivative term:

$$\Delta\theta_{p,des} = -K_p \cdot e_\tau - K_d \cdot \dot{\theta}_p \quad (5.13)$$

where K_p is a proportional gain, $e_\tau = \tau - \tau_{des}$ is torque error, τ is measured exoskeleton torque, τ_{des} is desired exoskeleton torque, K_d is a damping gain, and $\dot{\theta}_p$ is measured velocity of the motor pulley. In pilot testing, we found the damping term more effective than a term with the derivative of torque error; torque was measured with analog strain gauges, which included substantial noise, while pulley position was measured with a digital encoder. Damping was placed on motor pulley velocity alone rather than the relative velocity between the motor pulley and the exoskeleton joint. In pilot tests, using relative velocity was less effective, likely due to the irregular effects of stiction in the Bowden cable transmission on ankle joint velocity.

$L2$: Proportional Control with Damping Injection and Error-Dependent Gains (PD*+EDG)

This controller was identical to $L1$, with the exception that the proportional gain was error-dependent [60, 62], and increased with torque error:

$$\begin{aligned}K_p^* &= \min\left(\left\lceil \frac{|e_\tau|}{h_\tau} \right\rceil \cdot h_k, K_{max}\right) \\ \Delta\theta_{p,des} &= -K_p^* \cdot e_\tau - K_d \cdot \dot{\theta}_p\end{aligned}\quad (5.14)$$

where the symbol $\lceil \cdot \rceil$ denotes the *ceiling* operation, K_p^* is the error-dependent proportional gain, h_τ and h_k are torque error and proportional gain step sizes, and K_{max} is the maximum allowable gain. This is similar to

performing proportional control on the square of the torque error, with a sign and gain adjustment. This type of gain scheduling is expected to result in slower corrections, and fewer oscillations, when torque tracking errors are small.

L3: Proportional Control with Damping Injection and Previous-Error Compensation (PD*+PEC)

This controller was identical to *L1*, except that desired torque was altered based on torque error from the previous instant in time [86, 87] as:

$$\begin{aligned}\tau'_{des} &= \tau_{des} - e_{\tau,prev} \\ \Delta\theta_{p,des} &= -K_{pec} \cdot (\tau - \tau'_{des}) - K_d \cdot \dot{\theta}_p\end{aligned}\tag{5.15}$$

where τ'_{des} is the compensated torque error and $e_{\tau,prev}$ is the torque error from the previous time step. K_{pec} is a proportional gain. This approach is expected to increase the control response to large errors. It bears some similarity to integral control, in that it includes a term on prior error, but differs in that only the prior error at the previous sampling time is used rather than the entire time history. In cases where torque error changes slowly, this approach approximates a doubling of the proportional gain.

L4: Proportional-Integral Control with Damping Injection (PID*)

This controller was analogous to classical proportional-integral-derivative control, with damping injection substituted for the derivative term:

$$\Delta\theta_{p,des} = -K_p \cdot e_{\tau} - K_i \cdot \int_{t_0}^t e_{\tau} dt - K_d \cdot \dot{\theta}_p\tag{5.16}$$

where K_i is the gain on the integral of torque error, t_0 is the time at which the stride began, and t is the present time. Integral control is expected to eliminate steady-state error by accumulation of control input [35, 36, 50].

Model-Based Feed-Forward Control

Many systems with series elastic actuators use an inverse dynamics model of the series spring as a feed-forward control element, typically added to a model-free feedback component. We implemented one such model-based controller in this study, *L5*.

L5: Proportional Control with Damping Injection and Model-based Compensation (PD*+M)

This controller included both the classical feedback controller of *L1* and a model-based feedforward term, which was intended to anticipate changes in desired motor position due to either changes in exoskeleton joint angle or changes in desired joint torque:

$$\begin{aligned}\Delta\theta_{p,des} &= -K_p \cdot e_{\tau} - K_d \cdot \dot{\theta}_p + (\theta_{mdl} - \theta_p) \\ \theta_{mdl} &= \theta_e \cdot \tilde{R} - \tau_{des} \cdot \tilde{K}_t^{-1}\end{aligned}\tag{5.17}$$

where θ_{mdl} is a model-based motor position compensation generated from Eq. (5.6), θ_p is measured motor pulley position, θ_e is measured exoskeleton ankle joint angle, \tilde{R} is the estimate of R as defined in Eq. (5.5), or the ratio of the exoskeleton lever arm to the motor pulley radius, and \tilde{K}_t is an estimate of K_t , which is the total stiffness of the tether, series spring, and other structures between the motor pulley and exoskeleton joint as defined by Eq. (5.7). This is an inverse dynamics approach similar to computed torque and feedback linearization in nonlinear control. If desired torque remains constant but the exoskeleton joint moves, we expect the motor to need to move in proportion. If the joint is stationary but desired torque changes, we expect we know how much to move the motor to obtain the desired change in torque.

We also performed pilot tests with a version of this controller in which change in pulley angle, rather than absolute pulley angle, was anticipated based on the rate of change in exoskeleton angle and the rate of change in desired torque. This approach was less stable, owing to the effects of Bowden cable stiction on exoskeleton joint angle and the interplay between user behavior and desired torque through the high-level controller.

Model-Based Feedback Control

Adaptive control approaches [88, 89] using more complete system models have also been applied to exoskeletons. Such regimes have the capacity to exploit additional knowledge of system dynamics and allow theoretical tests of stability and performance. We developed a new adaptive controller for this system using a passivity-based approach, $L6$.

$L6$: Passivity-Based Adaptive Control (PAS)

Combining the dynamics of the subsystems described by Eqs. (5.1)–(5.8) so as to eliminate F and i_a , we have following dynamics of the system:

$$\ddot{\tau} + K_1 \dot{\tau} + K_2 \tau + S_\theta \dot{\theta}_e = K_V V_a + K_h \tau_h \quad (5.18)$$

in which τ denotes the torque transmitted to the exoskeleton from the motor, θ_e denotes the exoskeleton joint angle, V_a is the voltage applied to the armature of the motor, and τ_h denotes the torque applied to the exoskeleton by the human body. K_V , K_1 , K_2 and K_h are positive gains expressed as

$$\begin{aligned} K_V &= \frac{r_a r_p K_a K_c}{I_e N R_a} \\ K_1 &= \frac{1}{I_e} \left(\frac{K_a K_b}{R_a} + f_e \right) \\ K_2 &= \frac{r_p^2 K_c}{N^2 I_e} + \frac{r_a^2 K_c}{I_e} \\ K_h &= \frac{r_a^2 K_c}{I_e}, \end{aligned}$$

and S_θ is a gain expressed as

$$S_\theta = \left[\frac{r_a^2 K_c}{I_e} \left(\frac{K_a K_b}{R_a} + f_e \right) - \frac{r_a^2 K_c B_e}{I_e} \right]$$

with definitions of system constants provided in Section 5.2.1. Based on the system model in Eq. (5.18), we developed a new, provably stable, adaptive controller for the system.

We define the controller as:

$$\begin{aligned} V_a &= -K_p \cdot e_\tau - K_s \cdot s \\ &\quad + Y_d(\tau, \dot{\tau}_r, \ddot{\tau}_r, \dot{\theta}_e) \cdot \tilde{\Gamma} \\ &\quad - K_{sw} \cdot \text{sign}(s) \end{aligned} \quad (5.19)$$

where K_p and e_τ are as defined in $L1$, K_s is the sliding control gain, s is the sliding vector, defined below, Y_d is a regressor, defined below, Γ and $\tilde{\Gamma}$ are the system parameter vector and its estimate, defined below, and K_{sw} is the switching term gain. The sliding vector s is defined as:

$$s = \dot{\tau} - \dot{\tau}_{des} + \lambda \cdot e_\tau = \dot{\tau} - \dot{\tau}_r$$

where λ is a positive scalar and τ_r is a virtual reference torque. The regressor, Y_d , is defined as:

$$Y_d(\tau, \dot{\tau}_r, \ddot{\tau}_r, \dot{\theta}_e) = [\tau \quad \dot{\tau}_r \quad \ddot{\tau}_r \quad \dot{\theta}_e],$$

and is used to express the dynamics as a linear combination of system parameters as:

$$Y_d \cdot \Gamma = \frac{1}{K_V} \cdot \ddot{\tau}_r + \frac{K_1}{K_V} \cdot \dot{\tau}_r + \frac{K_2}{K_V} \cdot \tau + \frac{S_\theta}{K_V} \cdot \dot{\theta}_e$$

The system parameter, Γ , is defined as:

$$\Gamma = K_V^{-1} \cdot [1 \quad K_1 \quad K_2 \quad S_\theta]^T.$$

With full knowledge of system parameters, or $\tilde{\Gamma} = \Gamma$, Eq. (5.19) describes a model-based computed torque controller. For practical reasons, however, it is difficult to identify the value of Γ . Therefore, an update law is added to estimate the system parameters, $\tilde{\Gamma}$, as follows:

$$\dot{\tilde{\Gamma}} = -LY_d^T s. \quad (5.20)$$

where L is a symmetric positive definite parameter adaptation gain matrix. This parameter updating process reduces the model-dependency of the controller in Eq. (5.19), because only the structure of the dynamic model is used in the construction of the controller.

The closed-loop system with the model-based adaptive controller described by Eqs. (5.19)–(5.20) and dynamics described by Eq. (5.18) is stable and the exoskeleton torque trajectory τ converges to the desired value of τ_{des} , provided that the human input torque, τ_h , the desired torque trajectory, τ_{des} , and their time derivatives, $\dot{\tau}_h$, $\dot{\tau}_{des}$, and $\ddot{\tau}_{des}$, are bounded. A proof is provided in Appendix A.

In pilot tests, we found that better performance was obtained with this controller by setting the time rate of change in desired torque to zero. In practice, for most high-level controllers, the time derivative of desired torque, $\dot{\tau}_{des}$, could not be calculated in advance and contained substantial noise when approximated numerically. Noise on this signal arose from the human measurements used by the high-level controllers to calculate desired torque. We also found that the time derivative of torque error, \dot{e}_τ , contained substantial noise, in part due to noise on the analog strain gauge signal and in part due to complex Bowden cable transmission dynamics. Better performance was obtained using motor output pulley velocity, $\dot{\theta}_p$, in its place. This substitution is equivalent to assuming that the characteristic time of exoskeleton joint dynamics was much larger than the characteristic time of motor dynamics (Eq. 5.6). It is also analogous to the use of damping injection in place of derivative control in the other controllers tested. The sliding vector and regressor are therefore approximated as:

$$\begin{aligned} s &\approx \dot{\theta}_p + \lambda \cdot e_\tau \\ Y_d &\approx [\tau - \lambda \cdot e_\tau - \lambda \cdot \dot{\theta}_p \quad \dot{\theta}_e] \end{aligned}$$

Additionally, in pilot tests we found that it was more effective to operate the dedicated motor drive in velocity control mode, rather than voltage control mode. This difference in performance is likely due to the faster control loop in the motor driver, which allowed voltage to be changed more frequently and with less delay than for the control system as a whole. Motor velocity is strongly related to applied voltage, since the two are linearly related for a given torque at steady state (Eq. 5.11). This led to a similar formulation as for all other low-level controllers:

$$\begin{aligned} \Delta\theta_{p,des} &= -K_p \cdot e_\tau - K_s \cdot s \\ &\quad + Y_d(\tau, e_\tau, \dot{\theta}_p, \dot{\theta}_e) \cdot \tilde{\Gamma} \\ &\quad - K_{sw} \cdot \text{sign}(s) \end{aligned} \quad (5.21)$$

Model-Free Feed-Forward Control

We also tested a group of controllers that use iterative learning as a feed-forward component, which were expected to improve performance by exploiting the cyclic nature of human gait.

L7: Iterative Learning of Desired Motor Position (LRN)

This controller used torque error at each instant of one stride to update a feed-forward trajectory of desired motor position for each instant of the next stride. This is a variation on iterative learning, which, more generally, exploits the cyclic nature of a task to compensate complex system dynamics without an explicit model [90–93]. While walking is not as consistent as the operations of most industrial robots, it is cyclic, which was expected to afford some improvement in torque errors that occurred consistently from stride to stride.

The feed-forward trajectory of desired motor position, $\theta_{p,des}$, was calculated as:

$$\theta_{p,des}(i, n+1) = \theta_{p,des}(i, n) - K_I \cdot e_\tau(i, n) \quad (5.22)$$

where i is the time index or number of control cycles elapsed within this stride, n is this stride and $n + 1$ is the next stride, and K_I is the iterative learning gain. Desired motor position was then enforced as:

$$\Delta\theta_{p,des}(i,n) = \theta_{p,des}(i+D,n) - \theta_p(i,n) \quad (5.23)$$

where D is an estimate of the delay between commanding and achieving a change in motor position. During tuning, both K_I and D were adjusted.

Current torque error thereby updates desired motor position for the same time index on the next stride, while commanded motor velocity at this time index is based on a preview of desired motor position later in the same stride. Since the learned trajectory used in the present step has no dependence on the present torque, this method is feed-forward. However, present motor pulley position measurements were used in generating present motor velocity commands. This method can therefore be viewed as a feed-forward iterative learning control of torque combined with proportional feedback control of motor position.

Forgetting during Learning

To avoid divergence due to excessive accumulation of ripples during the learning process, a ‘forgetting’ constant was introduced to Eq. (5.22) as:

$$\theta_{p,des}(i,n+1) = \beta \cdot \theta_{p,des}(i,n) - K_I \cdot e_\tau(i,n) \quad (5.24)$$

where $\beta \in [0, 1]$ is a weight on the learned trajectory. For $\beta = 1$, all learning is retained, zero steady-state offset is expected, but ripples can form if the value of D is incorrect. For $\beta < 1$, torque errors from strides before the last stride have a reduced effect on controller behavior, reducing likelihood of ripple formation, but leading to some steady-state torque offset. For $\beta = 0$, iterative learning is disabled. $L7$ then becomes proportional control based on the torque error delayed by one step, and poor torque tracking performance is expected.

Learning from Filtered Errors

Noise in the error signal leads to inappropriate updates on the learned trajectory, which can excite unstable ripple formation. This excitation can be reduced by filtering the error signal across strides:

$$e_{flt}(i,n) = (1 - \mu) \cdot e_{flt}(i,n-1) + \mu \cdot e_\tau(i,n) \quad (5.25)$$

where e_{flt} is the filtered torque error trajectory, initially an array of zeros, used in place of e_τ in Eq. (5.22) and (5.24), and $\mu \in [0, 1]$ is a weighting term on the learned error. For $\mu = 1$, only the error from the last stride is used to update the motor trajectory, resulting in faster convergence but larger effects of sensor noise. For $\mu < 1$, errors at this time increment from all prior strides have some effect on the motor trajectory update, resulting in slower but more stable convergence. For $\mu = 0$, torque error is not updated, and iterative learning is disabled.

$L8$: Iterative Learning of Desired Motor Position + Proportional-Damping Compensation (LRN+PD*)

This controller combined iterative learning with proportional-damping feedback control to compensate remaining torque errors. It is a direct superposition of controllers $L1$ and $L7$, in which the absolute desired motor position was learned as in $L7$ and feedback control was applied as in $L1$:

$$\begin{aligned} \theta_{p,des}^{LRN}(i,n+1) &= \beta \cdot \theta_{p,des}^{LRN}(i,n) - K_I \cdot e_{flt}(i,n) \\ \theta_{p,des}(i,n) &= \theta_{p,des}^{LRN}(i+D,n) \\ &\quad - K_p \cdot e_\tau(i,n) - K_d \cdot \dot{\theta}_p(i,n) \\ \Delta\theta_{p,des}(i,n) &= \theta_{p,des}(i,n) - \theta_p(i,n) \end{aligned} \quad (5.26)$$

Combining iterative learning with feedback control is thought to result in improved performance compared to either component used in isolation [44]. Iterative learning is expected to generate a feed-forward trajectory that tracks torque for an average stride with zero steady-state error regardless of the complexity of the command signal required, but to be susceptible to step-by-step variability. Proportional-damping control is expected to quickly compensate for small torque errors, but to be susceptible to rapid changes in desired or measured torque.

L9: Proportional Control with Damping Injection + Iterative Learning Compensation (PD*+ΔLRN)

This controller is another combination of proportional-damping feedback and iterative learning feed-forward control elements. Unlike controllers $L7$ and $L8$, the values to be learned are desired changes in motor position instead of absolute desired positions:

$$\begin{aligned}\Delta\theta_{p,des}^{LRN}(i,n+1) &= \beta \cdot \Delta\theta_{p,des}^{LRN}(i,n) - K_I \cdot e_{flt}(i,n) \\ \Delta\theta_{p,des}(i,n) &= -K_p \cdot e_\tau(i,n) - K_d \dot{\theta}_p(i,n) \\ &\quad + \Delta\theta_{p,des}^{LRN}(i+D,n)\end{aligned}\tag{5.27}$$

This controller is very similar to $L8$, and is expected to have similar strengths and weaknesses. Differences in motor position are learned rather than absolute positions, however, which eliminates measured motor pulley position, θ_p , from the formulation. It is therefore a velocity control approach rather than a position control approach. This may affect stability, drift and the level and source of noise in the learned trajectory, which may in turn affect the allowable gains and speed of convergence. Learning desired changes in position also affects interactions between the feedback and feed-forward elements of the controller in the presence of step-by-step variability; learned changes in position add the same way regardless of present position and error, while the contribution of learned absolute positions depends upon the present motor position. Either approach can oppose feedback contributions under some conditions, but in different ways. A detailed mathematical comparison of these two approaches is provided in Appendix B.

Additional Feedback Control Terms Piloted

Several control elements that seemed likely to improve performance in theory did not fare well in pilot tests. This may be due to the unique features of the control problem at hand, in particular the noisy sensory information and the complex, changing dynamics of both the Bowden cable transmission and the human. These approaches were not included in the final data collection.

One such example is the traditional derivative control element

$$-K_d(\dot{\tau} - \dot{\tau}_{des})$$

which involves the derivative of torque error. Analog noise in the derivative of measured torque limited the magnitude of the derivative gain that could be applied without causing oscillations. This limited the capacity of the derivative term to stabilize the system, in turn limiting the magnitude of the proportional gains that could be applied.

Using the model described by Eq. (5.6), we next approximated the derivative term as:

$$-K_d [(\dot{\theta}_p - \dot{\theta}_e R) - \dot{\tau}_{des} \cdot \tilde{K}_t]$$

where the relative velocity between the motor and exoskeleton was substituted for the noisy measured torque derivative. The derivative of desired torque is also problematic, however, because it generally cannot be calculated in advance and its numerical approximation online is subject to noise from the human measurements used by the high-level controller to calculate desired torque, for example electromyographic measurements.

We next tried using just the relative velocity between the motor pulley and exoskeleton joint:

$$-K_d(\dot{\theta}_p - \dot{\theta}_e R)$$

which is equivalent to making the additional approximation that the derivative of desired torque, $\dot{\tau}_{des}$, is negligible. However, this control element was also found to be ineffective in pilot tests due to noise on the derivative of the exoskeleton joint angle, which seems to primarily arise from stiction in the Bowden cable transmission.

Finally, we arrived at the simple damping term

$$-K_d \dot{\theta}_p$$

which relied only upon the derivative of motor pulley position, which had little noise to amplify, and provided sufficient damping to improve stability.

We also pilot tested proportional control without a damping term, which was effective. However, the addition of some damping always allowed for higher proportional gains and improved tracking performance. Therefore, proportional control was always used together with damping injection in our tests.

5.3.3 High-Level Assistance Controllers

Stance Torque Control

During the stance period, desired exoskeleton joint torque was set according to one of four high-level assistance controllers, $H1$ - $H4$, described below.

$H1$: Time Based Desired Torque Trajectory (TIME)

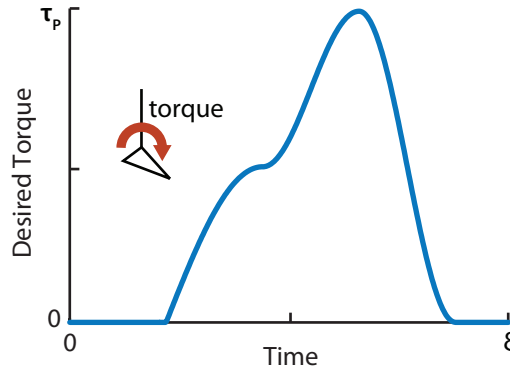


Figure 5.6: High-level control based on a trajectory in time

This high-level controller set desired torque as a function of time. Time-based control elements are simple and easily understood, and have been incorporated into many exoskeleton systems [22, 66, 67, 94]. We used a curve that resembled a scaled-down version of the human ankle moment during unassisted walking, calculated as:

$$\tau_{des} = \begin{cases} 0 & 0 < t < 0.15\xi \\ \frac{\tau_p}{2} \sin\left(\frac{t-0.15\xi}{0.3\xi}\pi\right) & 0.15\xi < t < 0.30\xi \\ \frac{-\tau_p}{4} \cos\left(\frac{t-0.3\xi}{0.15\xi}\pi\right) + \frac{3\tau_p}{4} & 0.30\xi < t < 0.45\xi \\ \frac{\tau_p}{2} \cos\left(\frac{t-0.45\xi}{0.15\xi}\pi\right) + \frac{\tau_p}{2} & 0.45\xi < t < 0.60\xi \\ 0 & 0.60\xi \leq t \end{cases} \quad (5.28)$$

where t is the time since the current stride began, ξ is stride period and τ_p is peak torque. We used $\xi = 1.1$ s and $\tau_p = 45$ N·m in this experiment, which produced the desired torque profile shown in Fig. 5.6.

$H2$: Joint Angle Based Desired Torque (ANGLE)

This high-level controller set desired torque as a function of exoskeleton ankle joint angle and phase of the gait cycle. This approach is a subset of impedance control, and is similar to setting desired torque based on a phase variable rather than clock time. Variations have been employed in many assistive devices [26, 41, 95]. We used a piece-wise linear curve that resembled a scaled-down version of the human ankle moment during unassisted walking, calculated as:

$$\tau_{des} = \frac{\tau_i - \tau_{i-1}}{\theta_{e,i} - \theta_{e,i-1}} (\theta_e - \theta_{e,i-1}), \quad i = \{1, 2, 3, 4\}, \quad (5.29)$$

with curve parameter values as listed in Table 5.1.

Here, (θ_i, τ_i) defines a node in torque-angle space (Fig. 5.7). The node (θ_2, τ_2) marked the transition from the dorsiflexion phase, in which ankle velocity was negative, to the plantarflexion phase, in which ankle velocity was positive. Since the exact transition point varied on each stride, we used the angle and torque at the moment of transition, (θ'_2, τ'_2) , when calculating desired torque in the first portion of Plantarflexion.

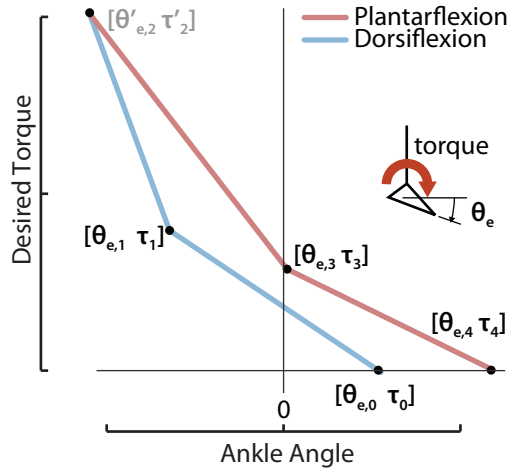


Figure 5.7: High-level control based on ankle joint angle

Table 5.1: Angle-based control parameter values

Param	Value	Param	Value
$[\theta_0, \tau_0]$	[0.018, 0.00]	$[\theta_3, \tau_3]$	[0.00, 11.3]
$[\theta_1, \tau_1]$	[-0.122, 18.1]	$[\theta_4, \tau_4]$	[0.140, 0.00]
$[\theta_2, \tau_2]$	[-0.209, 45.2]		

H3: Neuromuscular Model Based Desired Torque (NMM)

This high-level controller set desired exoskeleton torque based on a Hill-type muscle model and a positive force feedback reflex model. The resulting dynamics produce human-like motions and muscle activation patterns in simulation [96] and are thought to interact well with the human neuromuscular system [72–76]. Virtual muscle-tendon-unit length and velocity were set by measured exoskeleton joint angle and angular velocity. Virtual fiber length, velocity and activation were then used to determine muscle-tendon-unit force, F_{mtu} , which, after conditioning, was used to set desired exoskeleton torque. We conditioned the force signal by applying a low-pass filter with frequency ω_q , adding a small negative offset of τ_o^{nmm} , and applying a gain of K_{nmm} . Virtual muscle force was also used to drive a positive force feedback loop in which increased force led to increased muscle activation. The virtual neural system multiplied muscle force by a reflex gain, K_R , applied a time delay of D_R , added a small positive offset, $PreStim$, then applied a threshold, yielding the virtual muscle stimulation. Virtual muscle activation was driven by stimulation through first-order dynamics. A high-level schematic is provided in Fig. 5.8, high-level parameters are found in Table 5.2, and a full set of equations and parameters are available in Appendix C.

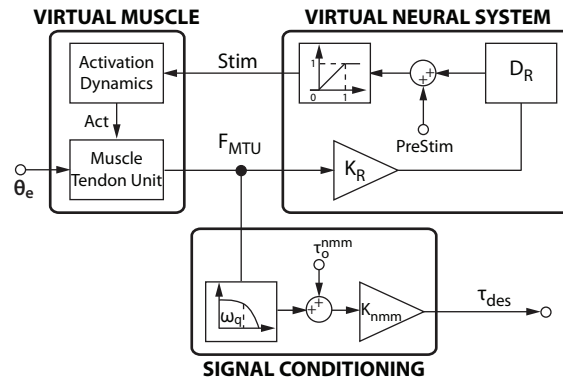


Figure 5.8: Neuromuscular model control schematic

Table 5.2: NMM parameter values

Param	Value	Param	Value
K_R	0.002	ω_q	50 Hz
D_R	0.020 s	τ_o^{nmm}	-20
$PreStim$	0.05	K_{nmm}	0.057 N·m

H4: Electromyography Based Desired Torque (EMG)

This high-level controller set desired torque in proportion to electromyographic measurements from the human gastrocnemius muscle. This approach gives the user direct neural control of the device, which is intended to make interactions more intuitive [47, 79, 80], but can result in more complex desired torque dynamics. Electrical activity in the gastrocnemius was measured using surface electrodes and a commercial electromyography system. The signal was then high-pass filtered at a frequency of ω_{hp} , rectified, and low-pass filtered at a frequency of ω_{lp} . A small negative offset, τ_o^{emg} , was applied, which prevented desired torque generation at low levels of muscle activity. The signal was then amplified by a gain, K_{emg} , yielding desired torque. A high-level schematic is provided in Fig. 5.9, and the parameters used in this experiment can be found in Table 5.3.

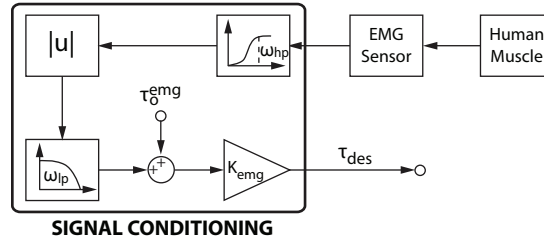


Figure 5.9: Proportional electromyography control schematic

Table 5.3: EMG parameter values

Param	Value	Param	Value
F_{hp}	20 Hz	F_{lp}	6 Hz
K_{emg}	283	τ_o^{emg}	-0.008

Swing Control

When the foot was off the ground, motor position control was employed to allow free motion of the human ankle and maintain a small amount of slack in the cable:

$$\begin{aligned}\theta_{p,des} &= \theta_e \cdot \tilde{R}, \\ \Delta\theta_{p,des} &= \theta_{p,des} - \theta_p\end{aligned}\tag{5.30}$$

where θ_e is exoskeleton joint angle and \tilde{R} is the estimated total gear ratio from motor to exoskeleton joint. Maintaining low slack in the Bowden cable reduced the time required for cable winding at the beginning of stance.

5.3.4 Experimental Methods

All experiments were conducted with one ($N = 1$) healthy adult participant (30 yrs, 56 kg, 1.65 m tall, female). Multiple participants were not warranted, as the aim of the study was to examine torque tracking performance by the exoskeleton, not biomechanical response of the human. The participant walked on a treadmill at $1.25 \text{ m}\cdot\text{s}^{-1}$ with a self-selected stride period of $1.08 \pm 0.06 \text{ s}$ while wearing the exoskeleton on one leg. The participant provided written informed consent prior to participation in the study, which was conducted in accordance with a protocol approved by the Carnegie Mellon University Institutional Review Board.

Before collecting data, we tuned parameters for each combination of high- and low-level controller as the participant walked with the exoskeleton. High-level control parameters listed in the prior section were selected so as to result in peak instantaneous desired torques of approximately 45 N·m during the course of one hundred steps of walking. Low-level control parameters listed in Table 5.4 were systematically tuned with the aim of minimizing torque error. Feedback, model and adaptive control gains in $L1-L6$ and $L8-L9$ were tuned using a variant of the Ziegler-Nichols method [97], in which:

1. All gains (proportional, damping, integral, model, sliding, and/or adaptive) were set to zero.
2. The proportional gain was increased until significant oscillations were observed.
3. Gain value and oscillation period were then recorded and used to estimate optimal values for proportional and damping gains.
4. Fine tuning of gains for all control elements, other than iterative learning, was then performed by the experimenter.

The iterative learning gain in $L7$ was tuned such that steady state was reached at approximately 10 strides, which led to a value of K_I that was about one tenth the tuned value of K_p . The same gains were used for iterative learning elements in controllers $L7-L9$. During tuning we found very similar suitable low-level control parameters across high-level controllers, and so used identical values within each low-level controller for consistency. Tuning was performed on a separate day from data collection. For model-based compensation, the value of \tilde{R} was based on measurements of the motor output pulley radius, motor gear ratio, and exoskeleton lever arm. \tilde{K}_c was estimated based on measurement of the passive relationship between exoskeleton torque and exoskeleton joint angle measured during walking experiments (Fig. 5.2).

Table 5.4: Low-level torque control parameter values

Param	Value	Param	Value	Param	Value
K_p	0.093	\tilde{R}	2.90	K_I	0.0077
K_d	0.010	\tilde{K}_c	195 N·m·rad ⁻¹	D	0.022 s
K_{max}	0.15	K_s	0.005	β	1
K_{pec}	0.046	λ	0.077	μ	1
K_i	7.7e-5	L	1.0e-9 I_3^*	T	0.250 s
h_τ	11.3 N·m	h_k	0.039	K_{sw}	0

(* I_3 denotes a 3×3 identity matrix)

For each high-level controller, all low-level control conditions were tested on the same day, without removal of the exoskeleton between trials. A table of condition order is presented in Supporting Materials¹ Table SI.

For each combination of low-level torque control and high-level assistance control, we collected data from 100 steady-state strides. Steady state was typically reached after about 20 strides. The subsequent 100 strides were then decomposed into individual strides, each beginning at heel strike as detected by a shoe-embedded switch. Data for an average stride were then calculated by taking the mean for each instant within the stride, in time, beginning at heel strike.

For each condition, we calculated torque error both for the set of all steady-state strides and for the average stride. We quantified torque error as the root mean squared error of the difference between measured and desired torque. For the set of all steady-state strides, we calculated root mean squared error for each stride individually, then calculated the mean and standard deviation. For the set of all steady-state strides, we compared means within high-level controllers and across low-level controllers using unpaired t-tests, with a significance level of $\alpha = 0.05$.

5.3.5 Results

Means and standard deviations of stride-wise root-mean-squared torque error (RMS-E) and average-stride root-mean-squared error (RMS-E AVG) of all low- and high-level controller combinations are shown in Fig. 5.10. A complete

¹The supporting document of this chapter is located at http://biomechanics.cit.cmu.edu/publications/Zhang_2016.BLL---SuppMat.pdf

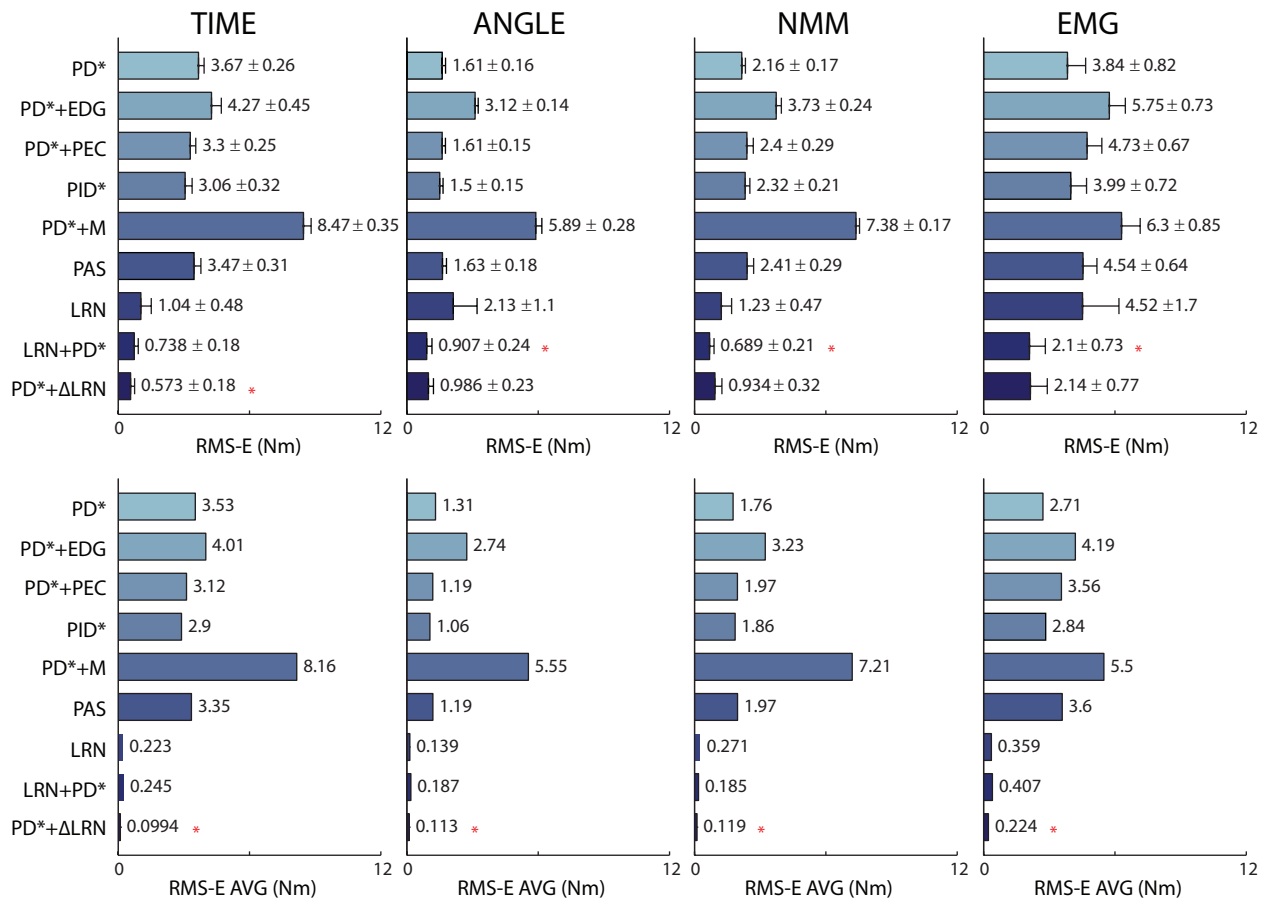
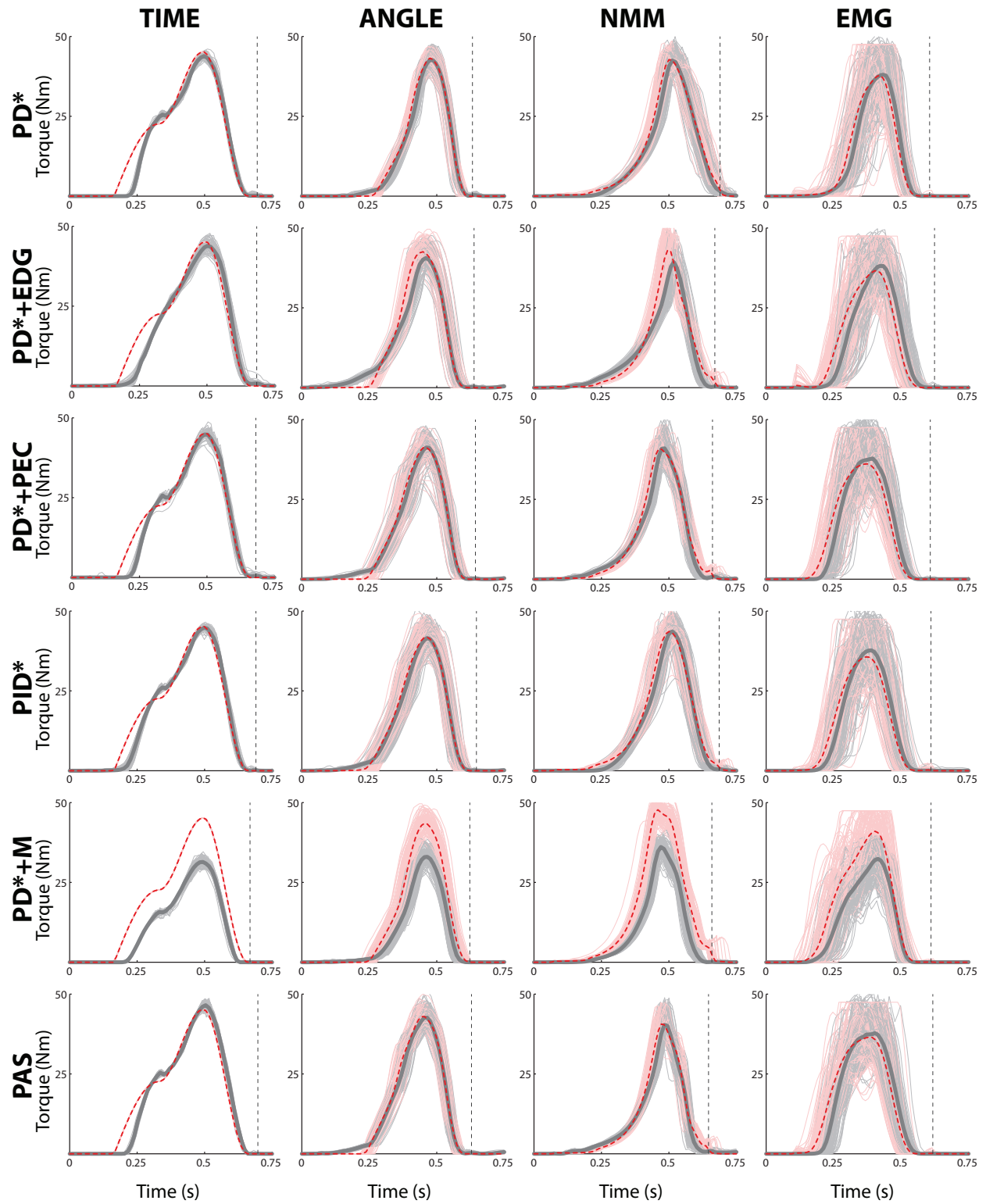


Figure 5.10: Root-mean-squared torque error calculated for all strides (RMS-E) and for an average stride (RMS-E AVG) across all high- and low-level control combinations.

table of p values for statistical comparisons between the RMS-E of all torque controllers are provided as Supporting Materials (Tables SII-SV). Overlapped time trajectories of desired and measured joint torques across all one hundred steady-state strides in each condition are shown in Fig. 5.11. Ankle angle trajectories in time and torque trajectories in ankle angle space are also provided for all conditions as Supporting Materials (Figs. S1-S2). Convergence plots for controllers that involved iterative learning are provided as Supporting Materials (Fig. S4).

The combination of proportional control and damping injection with iterative learning (PD*+ΔLRN or LRN+PD*) resulted in the lowest torque tracking errors for all high-level controllers, both in real-time and for average trajectories (Fig. 5.10). Of these two combinations with comparable performance, feedback control with learning compensation (PD*+ΔLRN) was simpler and converged faster. Stride-wise torque errors with PD*+ΔLRN were between 38% and 84% lower than with PD* alone ($p < 1.9 \cdot 10^{-43}$), while average-stride torque errors were between 91% and 97% lower, depending on high-level controller. Iterative learning control alone tended to result in low errors for average trajectories, but higher real-time errors than when combined with feedback control. Other additions to feedback control had minor effects on performance, except for model-based compensation, which increased torque error substantially. When desired torque was based on EMG, torque tracking error and variability were higher for almost all torque controllers. Values for the PD*+ΔLRN controller, including errors as a percentage of the maximum of the average desired torque, are provided in Table 5.5. The contributions of each component of the PD*+ΔLRN controller to desired motor displacement, and their evolution in time, are depicted in Fig. 5.12.

There were some interactions between high-level control type and low-level torque control performance. With Angle and EMG based high-level controllers, pure feedback control was more effective than pure iterative learning control, while for Time and NMM based controllers this trend was reversed. With Time-based desired torque, all controllers that did not have a learning component had poor tracking at the onset of desired torque, including a delay and overshoot, that comprised a large portion of the total torque error (Fig. 5.11). The addition of iterative learning to PD* control led to the greatest reductions in torque errors when desired torque was based on Time. An integral term



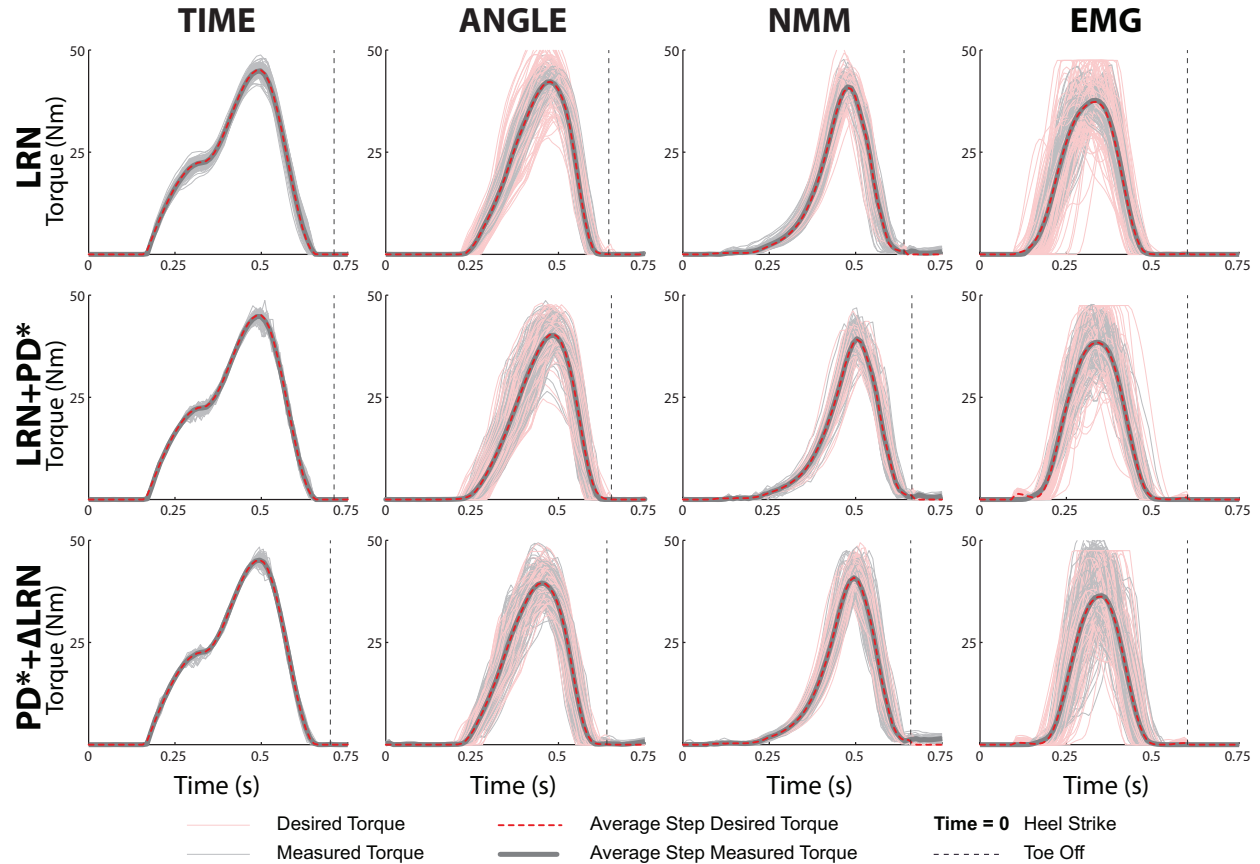


Figure 5.11: Time trajectories of desired torque (pink dots) and measured torque (gray dots) for 100 strides of walking, and average-stride desired torque (red line) and measured torque (gray line), for all combinations of controllers.

(PID*) provided a small improvement in performance over PD* control for Time and Angle based controllers. With Time-based high-level controllers, passivity (PAS) and previous-error compensation (PD*+PEC) provided a small benefit as well.

Table 5.5: Tracking errors with PD*+ΔLRN torque control for all four high level controllers

	RMSE	$\% \tau_{max}$	RMSE-A	$\% \tau_{max}$
Time	0.57 ± 0.18 Nm	1.3%	0.10 Nm	0.2%
Angle	0.99 ± 0.23 Nm	2.5%	0.11 Nm	0.3%
NMM	0.93 ± 0.32 Nm	2.3%	0.12 Nm	0.3%
EMG	2.14 ± 0.77 Nm	5.9%	0.22 Nm	0.6%

5.4 Discussion

In this study, we investigated the effectiveness of several prominent torque control techniques in robotic legged locomotion, implemented on a tethered ankle exoskeleton, with unidirectional series-elastic actuation, during human walking, with a variety of high-level assistance controllers. We found that model-free proportional control with damping injection compensated by iterative learning (Fig. 5.13) resulted in the lowest torque errors for all high-level controllers, both in real-time and for an averaged trajectory. This controller resulted in improved normalized torque tracking errors compared to prior torque control techniques.

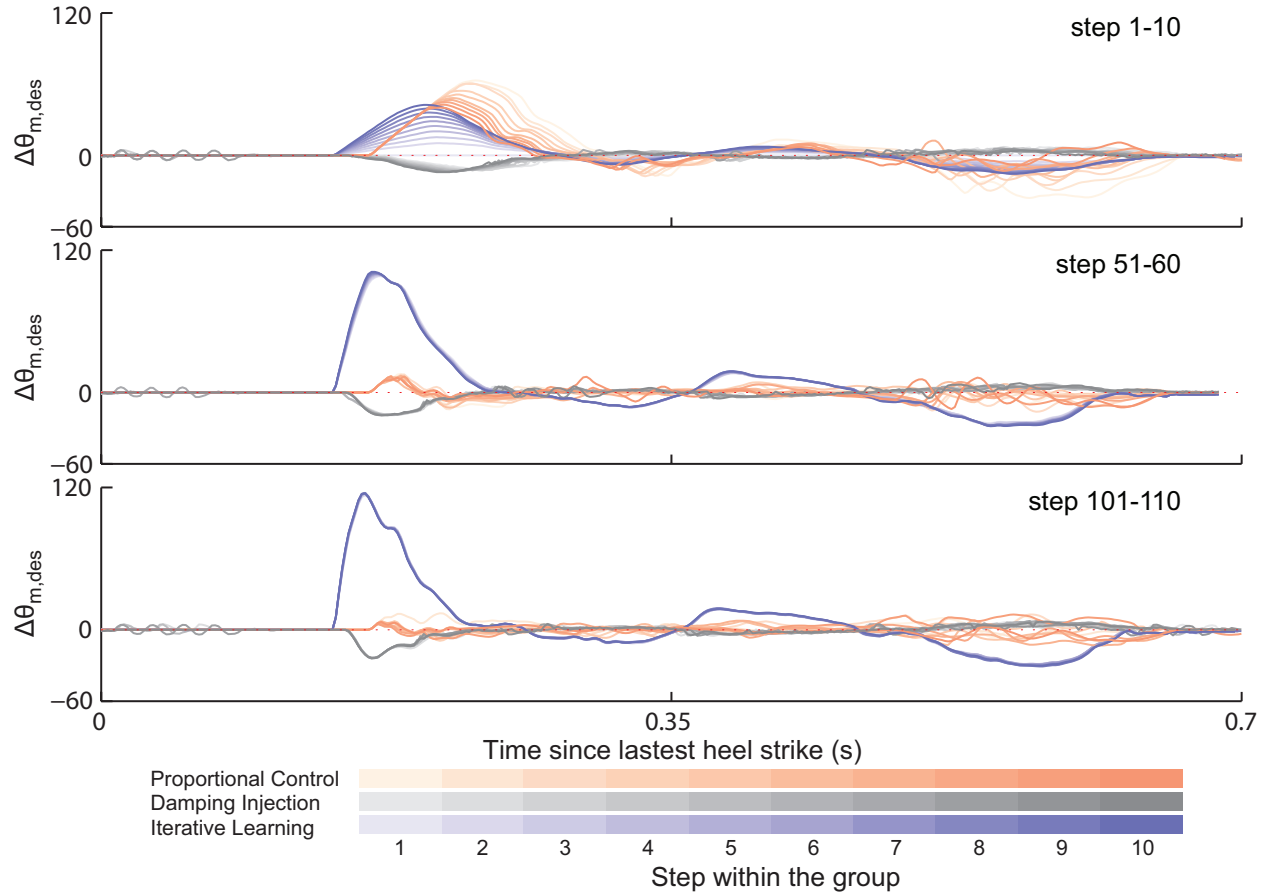


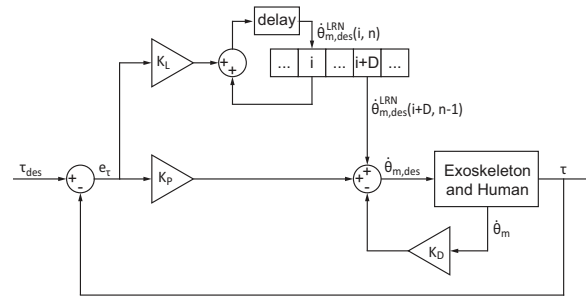
Figure 5.12: The contributions of each component of the PD*+ Δ LRN controller at steps 1-10, steps 51-60 and steps 101-110. In the first step proportional control dominates, and at steady state the learned component dominates. Data shown are from the Time-based high-level controller. Plots for all high-level conditions are available as Supplementary Materials (Fig. S5).

5.4.1 Proportional-learning-damping control

The most successful controller identified in this study has features that are analogous to those of classical proportional-integral-derivative control: a proportional term provides tracking during transients, iterative learning eliminates steady-state cyclic errors, and damping injection provides stability. We might therefore label the approach 'proportional-learning-damping' control.

Each component of the proportional-learning-damping controller contributes to overall commands in different ways across the learning process. During the first few walking steps, proportional control is the primary contributor, moderated by damping injection, while the learned trajectory remains near its initial value (Fig. 5.12, steps 1-10). At steady state, inputs are primarily the result of learned trajectories, which anticipate and override damping injection, while proportional control compensates for step-by-step variations in required input (Fig. 5.12, steps 91-100). This results in strong performance during transients and exceptional performance at steady state.

Designing and tuning the proportional-learning-damping controller in the form of Eq. (5.27) is straightforward. First, the proportional gain on torque error K_p is slowly increased until some overshoot and oscillations are observed. Next, the damping gain on motor velocity K_d is increased until high-frequency motor oscillations are observed, and the gain is backed off of this limit. The proportional gain is then re-tuned such that it is as high as possible without resulting in oscillations in torque error. Next, the learning gain K_l is set to a value of one tenth that of the proportional gain and fine-tuned until convergence occurs within the desired time, in this case about ten strides. Finally, a parameter sweep is performed on the delay parameter D used to preview learned desired motor position. The effects of learning

Figure 5.13: A block diagram of controller $L9, PD^*+\Delta LRN$

are sensitive to this choice; without a delay value very close to optimal, ripples in the learned desired motor position will form and grow. In those cases, non-unity values of the forgetting and error filtering terms, i.e., $\beta \neq 1, \mu \neq 1$ are required to stabilize the system. With the correct choice of delay, however, ripples did not form during at least one thousand strides in our experiments, even without forgetting or error filtering terms. We expect that a similar tuning process would be effective for a wide variety of lower-limb robotic systems used in legged locomotion.

This approach builds on the strengths of torque control techniques implemented in prior lower-limb exoskeletons and other legged locomotion robots. Feedback control terms similar to those tested in this study have been used in Bowden-cable driven hip-knee exoskeletons [40], hip-knee exoskeletons with collocated drives [43] and mobile hip exoskeletons [30]. Effective joint position tracking has been achieved in a knee exoskeleton using an iterative learning approach analogous to that tested in this study [65]. Improvements in torque tracking have been achieved in a Bowden-cable driven hip-knee exoskeleton using a lower-dimensional 'kernel-based' version of the iterative learning approach tested in this study [44]. The proportional-learning-damping controller identified in this study incorporates the most effective permutations of these previously-identified control concepts.

Comparisons to prior torque tracking results can be complicated by differences in hardware. For example, the present system has higher-power off-board motors than most exoskeletons, and the unidirectional Bowden cable can go slack during the swing phase, eliminating the need for active control to achieve transparency, i.e., the ability to apply zero impedance. On the other hand, some prior exoskeletons have estimated joint torques using simplified system models rather than direct measurement, which can result in the appearance of low-error torque tracking despite substantial unmeasured torque errors. Nevertheless, the proportional-learning-damping controller identified in this study achieved the lowest torque errors as a percentage of desired torque of any exoskeleton to date.

It is likely that iterative learning of the form used here or in other studies, would improve torque tracking during most human locomotor activities, since even irregular gaits exhibit some degree of repeatability. The case of the EMG-based high-level controller provides an insight into such scenarios, because the EMG signal contains substantial noise and is highly variable from step to step (Fig. 5.11; Fig. S2). Despite these irregularities, the addition of a learning component reduced torque tracking errors by 45% compared to feedback control alone in the EMG condition.

Further improvements in torque tracking for some high-level controllers might have been possible with alternate phase variables. Iterative learning resulted in the greatest improvements in torque tracking for the Time-based high-level controller, presumably because motor position adjustments were also learned in time. Learning as a function of ankle angle in the Angle condition, for example, might have resulted in greater improvements. On the other hand, time provides a unique and monotonically increasing phase variable, with consistent indexing across steps, capable of capturing control inputs with very high levels of complexity. This topic merits further exploration.

Although this case study was conducted on an ankle exoskeleton, the system characteristics that lead to the effectiveness of the proportional-damping-learning controller during torque tracking also apply to other robotic legged locomotion systems such as lower-limb prostheses and walking robots. The complex, uncertain and changing dynamics introduced by transmissions, gait variations, or human-robot interactions make model-based and continuous-time integral control actions ineffective. The cyclic behavior of walking leads to improved performance performance with the addition of an iterative learning element. The presence of delays leads to a benefit from a predictive feed-forward element, in this case a learned compensation. These factors are discussed in the following section.

5.4.2 Benefits of additional control elements

There appeared to be some interactions between high-level and low-level control elements, which might provide insights into strategies for circumstances that were not tested in this experiment.

Continuous-time integration

When proportional-damping control was augmented by an integral term (PID*), previous-error compensation (PD*+PEC), or passivity-based adaptation (PAS), torque error with Time-based high-level control was slightly improved. However, these continuous-time integral components showed no effect or negative effects in tracking performance for other high-level controllers. We can identify two factors that may explain the ineffectiveness of integral control in these cases. One factor is integral windup; the rapid changes in set point over the course of the stride could lead to either excessive or insufficient error accumulation. Another factor is the nonlinear, changing, delayed dynamics of the system; the Bowden cable has nonlinear stiffness, both the transmission and human change in time, and there are delays in the control loop and in motor actuation. All of these factors are known to limit integral control performance due to the linear accumulation of torque errors that are not linearly comparable [98]. In the case of the Time-based high-level controller, continuous-time integration may have been more effective due to the consistency of the desired torque in time, which may have translated into more constant torque errors than with other high-level controllers.

The apparent success of integral terms in other robotic legged locomotion systems with Bowden-cable transmissions may be due to differences in torque sensing, cable composition or activities tested. For example, controllers of the Lopes system have typically included an integral term on torque error [40, 44, 50]. Differences might relate to torque sensing. In the present study, torque was measured at the joint using strain gauges. In Lopes, torque has been estimated from relative angle of the motor and joint or from series spring deflection, which might result in a more linear relationship between motor angle input and apparent joint torque. Differences might also relate to hardware. The Bowden cables in Lopes have features that could make them more consistent with a simple spring model, such as stiffer, pre-stretched steel cables and bidirectional drives that do not allow slack. Differences might also relate to the characteristic behavior of the joint being assisted. Lopes assists the hip and knee, which have relatively smooth, continuous patterns of joint torque. In this study, we assisted the ankle joint, which typically involves sharper changes in dynamics. For example, the foot intermittently contacts the ground, discontinuously changing both the impedance of the ankle joint and the magnitude of desired torques. These changes connote rapid changes in set point for the controller, which leads to windup of integral control elements, among other challenges. The proportional-learning-damping controller developed here may therefore be expected to provide strong torque tracking performance under a larger range of conditions.

Model-based control elements

Although model-based control elements show promise in simulation and in theory, these generally worsened or had no effect on tracking performance in our experiment. One might expect that better performance could have been obtained with a more accurate estimate of model parameters in the PD*+M controller. However, in exploratory tests we found that the best performance was obtained by driving model-based contributions to zero. One reason for the ineffectiveness of model-based compensation may have been the nonlinear stiffness of the Bowden cable, which we modeled as a linear spring, and slow changes in cable stiffness and length due to heating over the course of each trial. Another reason may have been the exclusion of friction and stiction. However, in pilot tests using model-based compensation that included these elements, we found them to make the controller less robust; in each case the effects were highly sensitive to choice of parameter value and torque tracking error was not reduced. Sensitivity to model errors seems to be a fundamental issue in implementing this type of inverse-model control in devices with Bowden cable transmissions.

The passivity-based controller (PAS) fared slightly better, perhaps due to its adaptive nature, but still did not yield substantial benefits. One factor that may have limited its effectiveness is input mismatch; the controller was designed with motor voltage as input (Eq. 5.18), but implemented using motor velocity commands instead. While these terms are closely related (Eq 5.11), it is possible that an alternate mode of motor control, or an alternate formulation, could have led to improved results. Another factor that may have limited performance was the inclusion of a term akin to continuous-time integration, which is subject to windup as discussed above. The primary limitations likely stem from the reliance on any explicit model, however, since the dynamics of this human-robot system are highly complex and time-varying.

Some prior controllers have used model-based control elements, apparently to good effect. For example, [43] used continuous-time integration and model-based terms that were not found to improve performance in the present study. This may be because the Bowden cable transmission used here relocated heavy actuators off of the leg, making gravity compensation unnecessary, but had more unmodeled dynamics than a gear train, making friction compensation less effective. The proportional-learning-damping controller described here resulted in lower torque tracking error than in

prior systems, suggesting improved performance might be achieved even in systems for which model-based control has been effective. The proportional-learning-damping controller described here resulted in lower torque tracking error than in prior systems, suggesting improved performance might be achieved even in systems for which model-based control has been effective.

Gain scheduling, optimal control, and learning

Error-dependent gains (PD*+EDG) did not provide benefits for any high-level controller. Lower gains when torque errors were low seem to have led to larger errors at other times, since the set point changed rapidly and there were substantial execution delays. Gain scheduling methods that instead use optimal control might improve torque tracking for this system, but such feedback control techniques would still be limited by communication and actuation delays. By contrast, iterative learning realizes another form of optimal control, but uses a feed-forward approach to overcome delays. The iterative learning controller developed here is a variation on one-dimensional root finding using Newton's method. The problem is to find the desired motor position ($L7$ and $L8$) or displacement ($L9$) for zero torque error, i.e., to solve the function:

$$e_{\tau}(\Delta\theta_{m,des}) = 0 \quad (5.31)$$

The solutions are approximated in an iterative manner by

$$\Delta\theta_{m,des}(n+1) = \Delta\theta_{m,des}(n) - K_l \cdot e_{\tau}(n) \quad (5.32)$$

which can be rewritten as

$$\Delta\theta_{m,des}(n+1) = \Delta\theta_{m,des}(n) - \frac{e_{\tau}(\Delta\theta_{m,des}(n))}{K_l^{-1}} \quad (5.33)$$

This demonstrates a variation of Newton's method to solve $e_{\tau} = 0$ with the estimate for the derivative of e_{τ} fixed as $e'_{\tau} = K_l^{-1}$. Unlike gain scheduling in feedback control, this optimal control approach addresses control delays through the combination of a feed-forward term and a delay-compensating prediction term. Therefore, even with an optimized gain schedule, PD*+EDG probably would not out-perform PD*+ALRN.

5.4.3 Factors limiting interpretation

High-level controllers

It is difficult to make comparisons across high-level controllers for the same low-level torque controller, because tracking difficulty may vary with desired torque pattern. For example, we can imagine a Time-based trajectory with step changes in desired torque for which precise tracking would be infeasible. Similarly, the ease of tracking Angle-based desired torques likely depends on the similarities between the target torque-angle curve and the passive relationship arising from series elasticity. EMG-based desired torques generally seem to be difficult to track, given the unpredictable signals that directly drive desired torque, but increasing filter frequency could make this task easier. We did not test multiple values for high-level parameters in this experiment, which is an area for future work.

Interactions with human response

We designed this experiment with the implicit expectation that low-level torque control would not significantly affect human response to high-level assistance modes, but this does not appear to have been the case. Changes in the patterns of desired torque (Fig. 5.11) and joint kinematics (Supporting Materials, Section II) across torque controllers within the same high-level controller reveal an interaction effect. For example, we found more variability in joint kinematics with PD* torque control than with LRN torque control when desired torque was generated on the basis of Time. In this case, differences seem to be related to the smoothness of the measured torque generated by the two controllers; the subject reported that the PD* controller had uncomfortable oscillations, leading to compensatory activity, while the LRN controller did not. As another example, we found more variability in desired torque with NMM-based assistance than Angle-based assistance using PD* torque control, but an opposite trend using LRN torque control. This appears to

be the result of complex, multi-time-scale, dynamic interactions between continuous behavior of the torque controller, within-stride variations by the human, high-level control responses, and human adaptation over multiple strides. These effects may also be important in selecting and tuning an exoskeleton or prosthesis torque controller.

Hardware dependence

Robot hardware, particularly series compliance, also interacted with the quality of torque tracking. We performed pilot tests with no series spring, other than the Bowden cable, and found significant increases in torque error and subject discomfort for all control combinations. We also tried more compliant series springs, and found small increases in torque tracking error. When series stiffness is too high, we expect small position changes by the human to result in large, undesirable, changes in torque, and when it is too low we expect motor dynamics to limit performance [32]. Interactions between series elasticity, low-level torque control, high-level assistance, and assisted task should be explored in the future.

Some of the control elements found to be ineffective in this system might be more effective in devices with different hardware or task characteristics. For example, there are many examples of torque controllers incorporating model-based terms, often accompanied by hardware that lends itself more readily to modeling [e.g. 43]. Experimental comparisons of torque tracking performance with and without model-based terms in these systems would lend further insights into their potential contributions to effective torque tracking in exoskeletons and other robotic legged locomotion systems, and might provide a useful point of contrast to the present work. Future work could also address the effects of hardware changes as an additional dimension in the space sampled here. Measuring performance for each combination of a set of high-level controllers, low-level controllers and hardware setups would provide the best insights into interactions between these features. As the dynamical contributions of nonlinear time-varying elements, intermittent contact or forceful human interactions increase, continuous-time integral terms, gain scheduling, and model-based compensations are expected to become less effective, as observed with the unidirectional Bowden-cable-driven ankle-foot exoskeleton used in this study. The present system therefore represents a more challenging case for torque control, suggesting that the proportional-learning-damping controller identified here would perform even better in a system with simpler, more consistent dynamics.

The unidirectional Bowden cable used in this study made torque control more challenging, but is not the dominant factor in the observed patterns of torque error. The onset of applied torque tended to lag that of desired torque, particularly with feedback controllers and TIME based desired torque. This pattern might suggest that slack in the Bowden cable was the primary cause of torque error, but this is not the case. All high-level controllers set desired torque to zero during the beginning of stance, from about 0 to 0.25 s, consistent with typical human ankle torque patterns. All low-level controllers acted to track desired torque throughout stance, quickly eliminating slack from the previous swing phase early in the period of zero desired torque. The Bowden cable was therefore not slack upon the onset of desired torque. This is evident from the pattern of torque with feedback control and ANGLE based desired torque, which led desired torque beginning at about 0.10 s. Patterns in torque error across controllers are better-explained by a combination of rapid changes in desired torque, rapid movements of the human, and electromechanical delays in applying desired changes in motor position. These issues are common to most lower-limb exoskeletons, prostheses and walking robots, especially systems using series-elastic actuation.

5.4.4 Implications for control of future systems

The insights gained from this study are expected to help guide the design of torque controllers for systems with similar traits, particularly complex, changing dynamics and cyclic motions, such as lower-limb exoskeletons, active lower-limb prostheses and walking robots. Based on the present results, there is reason to expect that the combination of feedback control and feed-forward iterative learning, without continuous-time integration or model-based compensation, will provide strong torque tracking performance in any such system. Other control elements might further improve performance for some systems and control objectives. For example, if system dynamics are relatively constant and easy to identify, model-based compensation might be useful. If the measured and desired torque both change slowly, continuous-time integral control may also lead to some improvements. In any case, proportional-learning-damping control is expected to provide good baseline torque tracking.

5.5 Conclusions

We performed a systematic comparison of torque control techniques in a robotic legged locomotion system under realistic operating conditions, and found that the combination of proportional control, damping injection and iterative learning resulted in smaller torque errors relative to peak torque than any other approach tested or previously demonstrated. Designing this proportional-learning-damping controller was straightforward, requiring sequential tuning of only four parameters. Our results generally support such an approach for any torque-controlled lower-limb exoskeleton, prosthesis and walking robot. The complex interactions between device hardware, torque control, assistance control, task goals and human behavior, in case of exoskeletons and prostheses, remain a rich area for future research.

5.6 Acknowledgement

The authors thank Rachel Jackson and Kirby Witte for hardware assistance. This material is based upon work supported by the National Science Foundation under Grant No. IIS-1355716 and by the Singapore Economic Development Board NTU-CMU Dual PhD Scholarship.

Appendix A. Stability and Convergence of the Passivity Based Controller

Passivity

Substituting Eq. (5.19) into Eq. (5.18), we have the closed-loop equation:

$$\frac{1}{K_v} \dot{s} + \frac{K_1}{K_v} s + K_p e_\tau + K_s s + Y_d(\tau, \dot{\tau}_r, \ddot{\tau}_r, \dot{\theta}_e) \Delta\Gamma = \frac{K_h}{K_v} \tau_h. \quad (34)$$

in which $\Delta\Gamma = \Gamma - \tilde{\Gamma}$.

Let the output be $y = s$. Multiplying both side of Eq. (34) by the output and then integrating it, we have

$$\begin{aligned} & \int_0^t \frac{K_h}{K_v} s(\zeta) \tau_h(\zeta) d\zeta \\ &= \int_0^t \left[\frac{1}{K_v} s(\zeta) \dot{s}(\zeta) + \frac{K_1}{K_v} s^2(\zeta) + K_p \dot{e}_\tau(\zeta) e_\tau(\zeta) + K_p \lambda e_\tau^2(\zeta) + K_s s^2(\zeta) \right. \\ & \quad \left. + s(\zeta) Y_d(\zeta) \Delta\Gamma(\zeta) \right] d\zeta \\ &= \underbrace{P(t) - P(0)}_{\text{Stored Energy Change}} + \underbrace{\int_0^t W(\zeta) d\zeta}_{\text{Dissipated Energy}} \end{aligned}$$

in which the stored system energy is

$$P = \frac{1}{2K_v} s^2 + \frac{1}{2} K_p e_\tau^2 + \frac{1}{2} \Delta\Gamma^\top L^{-1} \Delta\Gamma \geq 0, \quad (35)$$

and the energy dissipating rate is

$$W = \left(\frac{K_1}{K_v} + K_s \right) s^2 + K_p \lambda e_\tau^2 \geq 0. \quad (36)$$

Since both V and W are non-negative, we can conclude the passivity of output y for the system (34).

With no disturbance from human, i.e., $\tau_h = 0$, we have

$$\dot{P} = -W.$$

Convergence

To compensate for non-zero human loading, $\tau_h \neq 0$, an additional switching term is added to the controller

$$V_a = -K_p e_\tau - K_s s + Y_d(\tau, \dot{\tau}_r, \ddot{\tau}_r, \dot{\theta}_e) \tilde{\Gamma} - K_{sw} \text{sign}(s) \quad (37)$$

where K_{sw} is the compensation gain. With Eq. (37), the closed loop system equation becomes

$$\begin{aligned} \frac{1}{K_v} \dot{s} + \frac{K_1}{K_v} s + K_p e_\tau + K_s s + Y_d(\tau, \dot{\tau}_r, \ddot{\tau}_r, \dot{\theta}_e) \Delta \Gamma \\ - \frac{K_h}{K_v} \tau_h + K_{sw} \text{sign}(s) = 0. \end{aligned} \quad (38)$$

The integral of the product of $y = s$ with the above equation is

$$\begin{aligned} \int_0^t \left[\frac{1}{K_v} s(\zeta) \dot{s}(\zeta) + \frac{K_1}{K_v} s^2(\zeta) + K_p \dot{e}_\tau(\zeta) e_\tau(\zeta) + K_p \lambda e_\tau^2(\zeta) \right. \\ \left. + K_s s^2(\zeta) + s(\zeta) Y_d(\zeta) \Delta \Gamma(\zeta) - s \frac{K_h}{K_v} \tau_h + s K_{sw} \text{sign}(s) \right] d\zeta \\ = \underbrace{P(t) - P(0)}_{\text{Stored Energy Change}} + \underbrace{\int_0^t W(\zeta) d\zeta}_{\text{Dissipated Energy}} \\ + \int_0^t \left[-s \frac{K_h}{K_v} \tau_h + s K_{sw} \text{sign}(s) \right] d\zeta \\ = 0, \end{aligned}$$

i.e.,

$$\dot{P} = -W + s \frac{K_h}{K_v} \tau_h - s K_{sw} \text{sign}(s). \quad (39)$$

Note that

$$\begin{aligned} s \frac{K_h}{K_v} \tau_h - s K_{sw} \text{sign}(s) &= s \frac{K_h}{K_v} \tau_h - K_{sw} |s| \\ &\leq \frac{K_h}{K_v} |s| k_0 - K_{sw} |s| \end{aligned}$$

where k_0 is a finite non-negative number defined by the boundedness of the human loading:

$$|\tau_h| \leq k_0.$$

By choosing a K_{sw} such that

$$K_{sw} \geq \frac{K_h}{K_v} k_0,$$

we have

$$s \frac{K_h}{K_v} \tau_h - s K_{sw} \text{sign}(s) \leq 0. \quad (40)$$

It is already established that

$$W \geq 0,$$

therefore, it is proved that

$$\dot{P} \leq 0.$$

Based on the non-negativeness of P and non-positiveness of \dot{P} , we have

$$P(t) \leq P(0),$$

i.e., $P(t)$ is bounded. Since P is quadratic on s , e_τ and $\Delta\Gamma$, these three terms are bounded. Eq. (39) means

$$P(t) - P(0) = - \int_0^t W(\zeta) d\zeta + \int_0^t \left[s(\zeta) \frac{K_h}{K_v} \tau_h(\zeta) - K_{sw} |s(\zeta)| \right] d\zeta. \quad (41)$$

Combining Eq. (41) with Eq. (40) and (36), we have

$$P(t) - P(0) \leq - \int_0^t W(\zeta) d\zeta \leq 0. \quad (42)$$

By definition, Eq. (36) and (42) lead to

$$s, e_\tau \in L_2(0, \infty). \quad (43)$$

Based on the definition of s , \dot{e}_τ is also bounded, and hence so is $\dot{\tau}$ since $\dot{\tau}_{des}$ is bounded. The boundedness of \dot{e}_τ proves the uniform continuity of e_τ .

Now due to the boundedness of $\dot{\tau}_{des}$ and $\ddot{\tau}_{des}$, $\dot{\tau}_r$ and $\ddot{\tau}_r$ are also bounded, which then lead to the boundedness of $Y_d(\tau, \dot{\tau}_r, \ddot{\tau}_r, \theta_e)$. Based on Eq. (38), \dot{s} is then bounded, which then proves the uniform continuity of s .

Combining the conclusions of uniform continuity, boundedness and Eq. (43), we have [99, 100]:

$$\begin{aligned} s &\rightarrow 0, \text{ as } t \rightarrow \infty, \\ e_\tau &\rightarrow 0, \text{ as } t \rightarrow \infty. \end{aligned}$$

By the definition of s and e_τ , we then can conclude

$$\begin{aligned} \tau &\rightarrow \tau_{des}, \text{ as } t \rightarrow \infty, \\ \dot{\tau} &\rightarrow \dot{\tau}_{des}, \text{ as } t \rightarrow \infty. \end{aligned}$$

i.e., both the actual ankle torque and its changing rate converge to the desired values.

Appendix C. PD*+ΔLRN versus LRN+PD*

For controller $L9$, i.e., PD*+ΔLRN, as described in Eq. (5.27), the total desired motor displacement at a certain time stamp t within step n , with a forgetting factor $\beta = 1$ and a filtering factor $\mu = 1$, is

$$\begin{aligned} \Delta\theta_{p,des}(n) \Big|_t &= \underbrace{\Delta\theta_{p,des}^{LRN}(0) \Big|_t - K_I \sum_{m=1}^{n-1} e_\tau(m) \Big|_t}_{\text{Step-wise Integral Control}} \\ &\quad \underbrace{- K_P e_\tau(n) \Big|_t}_{\text{Proportional Control}} \underbrace{- K_D \dot{\theta}_p(n) \Big|_t}_{\text{Damping Injection}} \end{aligned} \quad (44)$$

in which the operator

$$*(n) \Big|_t$$

denotes the variable $*$ at time t within step n , i.e., the time lapsed from the latest heel strike. The term

$$\Delta\theta_{p,des}^{LRN}(0) \Big|_t$$

denotes the initial value of the desired motor displacement to be learned. Iterative learning of desired motor displacement realizes a step-wise integral control action. Considering Eq. (44), it can be seen that $L9$ is analogous to traditional PID control; damping injection improves system stability in the manner of derivative control, and iterative learning takes eliminates steady-state errors across steps similar to integral control.

$$\begin{aligned}
\Delta\theta_{p,des}(n)\Big|_t &= \underbrace{\theta_{p,des}^{LRN}(0)\Big|_t - K_I \sum_{m=1}^{n-1} e_\tau(m)\Big|_t}_{\text{Step-wise Integral Control}} \underbrace{-K_P e_\tau(n)\Big|_t}_{\text{Proportional Control}} \underbrace{-K_d \dot{\theta}_p(n)\Big|_t}_{\text{Damping Injection}} \\
&\quad - \theta_p\Big|_0 \exp\left(-\frac{t}{T+K_d}\right) - \frac{1}{T+K_d} \int_0^t \exp\left(-\frac{t-\zeta}{T+K_d}\right) \left[\theta_{p,des}^{LRN}(0) - K_I \sum_{m=1}^{n-1} e_\tau(m)\Big|_\zeta - K_P e_\tau(n)\Big|_\zeta \right] d\zeta
\end{aligned} \tag{43}$$

For controller $L8$, LRN+PD*, combining Eqs. (5.26) and (5.12), we have

$$\begin{aligned}
\dot{\theta}_{p,des}(n)\Big|_t &= \frac{1}{T} \Delta\theta_{p,des}(n)\Big|_t \\
&= \frac{1}{T} \left[\theta_{p,des}^{LRN}(0)\Big|_t - K_I \sum_{m=1}^{n-1} e_\tau(m)\Big|_t - \theta_p(n)\Big|_t \right. \\
&\quad \left. - K_P e_\tau(n)\Big|_t - K_d \dot{\theta}_p(n)\Big|_t \right]
\end{aligned} \tag{37}$$

when $\beta = 1$ and $\mu = 1$.

Assuming perfect motor velocity tracking:

$$\dot{\theta}_p(n)\Big|_t = \dot{\theta}_{p,des}(n)\Big|_t \tag{38}$$

then Eq. (5.26) becomes

$$\begin{aligned}
\dot{\theta}_p(n)\Big|_t &= \frac{1}{T} \left[\theta_{p,des}^{LRN}(0)\Big|_t - K_I \sum_{m=1}^{n-1} e_\tau(m)\Big|_t - \theta_p(n)\Big|_t \right. \\
&\quad \left. - K_P e_\tau(n)\Big|_t - K_d \dot{\theta}_p(n)\Big|_t \right]
\end{aligned} \tag{39}$$

which can be written as

$$\begin{aligned}
\dot{\theta}_p(n)\Big|_t &= -\frac{1}{T+K_d} \theta_p(n)\Big|_t \\
&\quad + \frac{1}{T+K_d} \left[\theta_{p,des}^{LRN}(0)\Big|_t - K_I \sum_{m=1}^{n-1} e_\tau(m)\Big|_t \right. \\
&\quad \left. - K_P e_\tau(n)\Big|_t \right]
\end{aligned} \tag{40}$$

Assuming the same ankle kinematics for each step and the same motor position at each heel strike:

$$\theta_p(n)\Big|_0 = \theta_p\Big|_0,$$

the dynamics described in Eq. (40) can be treated as a linear-time-invariant system starting from the latest heel strike in the format of

$$\dot{x} = Ax + Bu \tag{41}$$

where x is $\theta_p(n)$, A is $-\frac{1}{T+K_d}$, and Bu is

$$\frac{1}{T+K_d} \left[\theta_{p,des}^{LRN}(0)\Big|_t - K_I \sum_{m=1}^{n-1} e_\tau(m)\Big|_t - K_P e_\tau(n)\Big|_t \right]$$

Therefore, the solution of LTI system as described in Eq. (40) is

$$\begin{aligned} \theta_p(n) \Big|_t &= \theta_p \Big|_0 \exp\left(-\frac{t}{T+K_d}\right) \\ &+ \frac{1}{T+K_d} \int_0^t \exp\left(-\frac{t-\zeta}{T+K_d}\right) \left[\theta_{p,des}^{LRN}(0) \Big|_t \right. \\ &\left. - K_l \sum_{m=1}^{n-1} e_\tau(m) \Big|_\zeta - K_p e_\tau(n) \Big|_\zeta \right] d\zeta \end{aligned} \quad (42)$$

in which t denotes the time lapsed since the last heel strike and $\zeta \in [0, t]$ is a variable tracing t .

Therefore, the control input of $L8$ can be expressed as in Eq. (43) (at the top of the current page). It can be seen that the LRN+PD* controller differs from the PD*+ΔLRN controller in that it has additional exponential and low-pass filtered continuous-time integral terms. These arise from the presence of $-\theta_p(n)$ in the control input.

This difference can also be illustrated in the frequency domain. The convolution term

$$\begin{aligned} &\int_0^t \exp\left(-\frac{t-\zeta}{T+K_d}\right) \left[\theta_{p,des}^{LRN}(0) \Big|_t \right. \\ &\left. - K_l \sum_{m=1}^{n-1} e_\tau(m) \Big|_\zeta - K_p e_\tau(n) \Big|_\zeta \right] d\zeta \end{aligned} \quad (44)$$

translates to

$$\frac{1}{s + \frac{1}{T+K_d}} \left[\theta_{p,des}^{LRN}(0) \Big|_s - K_l \sum_{m=1}^{n-1} e_\tau(m) \Big|_s - K_p e_\tau(n) \Big|_s \right] \quad (45)$$

in frequency domain. The low-pass filter term

$$\frac{1}{s + \frac{1}{T+K_d}}$$

realizes constant scaling at low frequency and integration at high frequency. Each evaluation of the term to be filtered,

$$\theta_{p,des}^{LRN}(0) \Big|_t - K_l \sum_{m=1}^{n-1} e_\tau(m) \Big|_t - K_p e_\tau(n) \Big|_t$$

is generated independently at the sampling frequency. Therefore, the term is expected to have high frequency. A continuous-time integration effect is therefore included in the control input with the LRN+PD* controller.

In our experimental comparison, we found that continuous-time integral action is not desirable due to the linear accumulation of terms that are not linearly correlated. Therefore, PD*+ΔLRN is preferred due to its simplicity and lack of continuous-time integration.

Appendix C. Neuromuscular Reflex Model

The neuromuscular model included a Hill-type muscle-tendon-unit (MTU) (Fig. 14), with total length, l_{mtu} , equal to the length of the series elastic element, l_{se} , plus that of the contractile element, l_{ce} . The length of the parallel elastic element, l_{pe} , was identical to l_{ce} . The total force produced by the MTU, F_{mtu} , was equal to the force on the series elastic element, F_{se} , and also equal to the sum of the contractile element force, F_{ce} , and the parallel elastic element force, F_{pe} (which was usually zero). The contractile element force was expressed as:

$$F_{ce} = f_L(l_{ce}) \cdot f_V(\dot{l}_{ce}) \cdot Act \cdot F_{max}$$

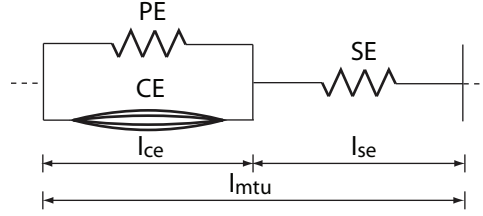


Figure 14: The Hill-type muscle-tendon-unit model includes a contractile element (CE), a parallel elastic element (PE) and series elastic element (SE).

in which $f_L(l_{ce})$ and $f_V(\dot{l}_{ce})$ are force scaling factors that reflect the force-length and force-velocity properties of muscle, Act is the muscle activation state, and F_{max} is the maximum force that can be produced by the muscle. The force-length and force-velocity relationships were:

$$f_L(l_{ce}) = \exp\left[-\frac{(l_{ce} - l_{ce,opt})^2}{(W \cdot l_{ce,opt})^2}\right],$$

and

$$f_V(\dot{l}_{ce}) = \begin{cases} A \frac{v_{max} + F_v^{max} \cdot \dot{l}_{ce}}{v_{max} \cdot A + \dot{l}_{ce}}, & \dot{l}_{ce} < 0 \\ \frac{v_{max} \cdot A + F_v^{max} \cdot (A + 1) \cdot (F_v^{max} - 1)}{v_{max} \cdot A + \dot{l}_{ce} \cdot (A + 1) \cdot (F_v^{max} - 1)}, & \dot{l}_{ce} \geq 0. \end{cases}$$

in which $l_{ce,opt}$ is the optimal contractile element length, W is a force-length constant, \dot{l}_{ce} is the contractile element velocity, A is a force-velocity constant, v_{max} is the maximum contraction velocity, and F_v^{max} is the maximum eccentric (lengthening) muscle scaling factor.

Series and parallel elastic element forces were determined as:

$$F_{se} = F_{max} \cdot \frac{1}{(u_{max} \cdot l_{se,sl})^2} \cdot \max(\delta l_{se}, 0)^2,$$

and

$$F_{pe} = \begin{cases} k_1 \cdot \delta l_{pe} + F_{max} \cdot \frac{k_{pe}}{l_{ce,opt}^2} \cdot \delta l_{pe}^2, & \delta l_{pe} > 0, \\ k_1 \cdot \delta l_{pe}, & \delta l_{pe} \leq 0. \end{cases}$$

where $\delta l_{pe} = l_{ce} - 1.5 \cdot l_{ce,opt}$ and $\delta l_{se} = l_{se} - l_{se,sl}$, and $l_{se,sl}$ is the slack length of the series elastic element, u_{max} is an elastic element curve parameter and k_1 is the sub-slack elastic element stiffness of the parallel elastic element.

The virtual muscle had activation dynamics as:

$$Act(t = 0) = PreAct,$$

$$Act = (Stim - Act) \cdot \left(\frac{Stim}{t_a} - \frac{1 - Stim}{t_d} \right)$$

where $Stim$ is neural stimulation from the positive reflex mechanism of the virtual neural system, t_a and t_d are muscle activation and deactivation time constants respectively, and the initial activation value $A(t = 0)$ is defined by $PreAct$.

The parameter values used in this study are listed in Table 6.

Table 6: Muscle model parameter values used in NMM

Param	Value	Param	Value
$l_{ce,opt}$	0.055 m	$l_{se,sl}$	0.245 m
$l_{mtu,0}$	0.284 m	F_{max}	1000 N
A	0.25	W	0.56
$F_{v,max}$	1.8	u_{max}	0.04
v_{max}	0.55 m/s	k_1	1
t_a	0.02 s	t_d	0.05 s
$PreAct$	0.05		

Bibliography

- [1] W. Cloud, "Man amplifiers: Machines that let you carry a ton," *Popular Science*, vol. 187, no. 5, pp. 70–73, 1965.
- [2] R. S. Mosher, "Handyman to hardiman," SAE Technical Paper, Tech. Rep., 1967.
- [3] A. A. Frank, "Automatic control systems for legged locomotion machines," DTIC Document, Tech. Rep., 1968.
- [4] S. Jezernik, G. Colombo, T. Keller, H. Frueh, and M. Morari, "Robotic orthosis lokomat: A rehabilitation and research tool," *Neuromodulation*, vol. 6, no. 2, pp. 108–115, 2003.
- [5] G. Aguirre-Ollinger, J. E. Colgate, M. A. Peshkin, and A. Goswami, "Active-impedance control of a lower-limb assistive exoskeleton," in *Proceedings of the IEEE/RSJ International Conference on Rehabilitation Robotics (ICORR)*. IEEE, 2007, pp. 188–195.
- [6] K. Suzuki, G. Mito, H. Kawamoto, Y. Hasegawa, and Y. Sankai, "Intention-based walking support for paraplegia patients with robot suit HAL," *Advanced Robotics*, vol. 21, no. 12, pp. 1441–1469, 2007.
- [7] B.-C. Tsai, W.-W. Wang, L.-C. Hsu, L.-C. Fu, and J.-S. Lai, "An articulated rehabilitation robot for upper limb physiotherapy and training," in *Proceedings of the IEEE/RSJ International Conference on Intelligent Robots and Systems (IROS)*. IEEE, 2010, pp. 1470–1475.
- [8] A. de Luca, A. Albu-Schaffer, S. Haddadin, and G. Hirzinger, "Collision detection and safe reaction with the DLR-III lightweight manipulator arm," in *Proceedings of the IEEE/RSJ International Conference on Intelligent Robots and Systems (IROS)*. IEEE, 2006, pp. 1623–1630.
- [9] S. Haddadin, A. Albu-Schaffer, A. De Luca, and G. Hirzinger, "Collision detection and reaction: A contribution to safe physical human-robot interaction," in *Proceedings of the IEEE/RSJ International Conference on Intelligent Robots and Systems (IROS)*. IEEE, 2008, pp. 3356–3363.
- [10] J. Hidler, D. Nichols, M. Pelliccio, K. Brady, D. D. Campbell, J. H. Kahn, and T. G. Hornby, "Multicenter randomized clinical trial evaluating the effectiveness of the Lokomat in subacute stroke," *Neurorehabilitation & Neural Repair*, vol. 23, no. 1, pp. 5–13, 2009.
- [11] S. Mochon and T. McMahon, "Ballistic walking: an improved model," *Mathematical Biosciences*, vol. 52, pp. 241–260, 1980.
- [12] T. McGeer, "Passive dynamic walking," *International Journal of Robotics Research*, vol. 9, no. 2, pp. 62–82, 1990.
- [13] S. Collins, A. Ruina, R. Tedrake, and M. Wisse, "Efficient bipedal robots based on passive-dynamic walkers," *Science*, vol. 307, no. 5712, pp. 1082–1085, 2005.
- [14] B. W. Verdaasdonk, H. F. J. M. Koopman, and F. C. van der Helm, "Energy efficient walking with central pattern generators: from passive dynamic walking to biologically inspired control," *Biological Cybernetics*, vol. 101, pp. 49–61, 2009.
- [15] A. J. Ijspeert, "Biorobotics: Using robots to emulate and investigate agile locomotion," *Science*, vol. 346, pp. 196–203, 2014.
- [16] J. R. Andrews and N. Hogan, "Impedance control as a framework for implementing obstacle avoidance in a manipulator," *Control of Manufacturing Processes and Robotic Systems*, ASME, pp. 243–251, 1983.
- [17] H. Kazerooni, J.-L. Racine, L. Huang, and R. Steger, "On the control of the berkeley lower extremity exoskeleton (BLEEX)," in *Proceedings of the IEEE International Conference on Robotics and Automation (ICRA)*. IEEE, 2005, pp. 4353–4360.
- [18] P. A. Lasota, G. F. Rossano, and J. A. Shah, "Toward safe close-proximity human-robot interaction with standard industrial robots," in *Automation Science and Engineering (CASE), 2014 IEEE International Conference on*. IEEE, 2014, pp. 339–344.
- [19] J. F. Veneman, R. Kruidhof, E. E. Hekman, R. Ekkelenkamp, E. H. Van Asseldonk, and H. Van Der Kooij, "Design and evaluation of the lopes exoskeleton robot for interactive gait rehabilitation," *Neural Systems and Rehabilitation Engineering, IEEE Transactions on*, vol. 15, no. 3, pp. 379–386, 2007.
- [20] G. S. Sawicki and D. P. Ferris, "Powered ankle exoskeletons reveal the metabolic cost of plantar flexor mechanical work during walking with longer steps at constant step frequency," *Journal of Experimental Biology*, vol. 212, no. 1, pp. 21–31, 2009.
- [21] A. H. Stienen, E. E. Hekman, H. ter Braak, A. M. Aalsma, F. C. van der Helm, and H. van der Kooij, "Design of a rotational hydroelastic actuator for a powered exoskeleton for upper limb rehabilitation," *IEEE Transactions on Biomedical Engineering*, vol. 57, no. 3, pp. 728–735, 2010.
- [22] P. Malcolin, W. Derave, S. Galle, and D. De Clercq, "A simple exoskeleton that assists plantarflexion can reduce the metabolic cost of human walking," *PLoS one*, vol. 8, no. 2, p. e56137, 2013.
- [23] R. J. Jackson and S. H. Collins, "An experimental comparison of the relative benefits of work and torque assistance in ankle exoskeletons," *Journal of Applied Physiology*, vol. 0, no. 0, pp. 00–00, 2015.
- [24] J. Pratt, P. Dilworth, and G. Pratt, "Virtual model control of a bipedal walking robot," in *Robotics and Automation, 1997. Proceedings., 1997 IEEE International Conference on*, vol. 1. IEEE, 1997, pp. 193–198.
- [25] S. Au, M. Berniker, and H. Herr, "Powered ankle-foot prosthesis to assist level-ground and stair-descent gaits," *Neural Networks*, vol. 21, no. 4, pp. 654–666, 2008.
- [26] F. Sup, H. A. Varol, J. Mitchell, T. J. Withrow, and M. Goldfarb, "Preliminary evaluations of a self-contained anthropomorphic transfemoral prosthesis," *IEEE Transactions on Mechatronics*, vol. 14, no. 6, pp. 667–676, 2009.
- [27] J. M. Caputo and S. H. Collins, "An experimental robotic testbed for accelerated development of ankle prostheses," in *Proceedings of the IEEE International Conference on Robotics and Automation (ICRA)*. IEEE, 2013, pp. 2645–2650.
- [28] H. Kawamoto, S. Taal, H. Niniss, T. Hayashi, K. Kamibayashi, K. Eguchi, and Y. Sankai, "Voluntary motion support control of robot suit HAL triggered by bioelectrical signal for hemiplegia," in *Proceedings of the IEEE International Conference of the Engineering in Medicine and Biology Society*. IEEE, 2010, pp. 462–466.

- [29] O. Unluhisarcikli, M. Pietrusinski, B. Weinberg, P. Bonato, and C. Mavroidis, "Design and control of a robotic lower extremity exoskeleton for gait rehabilitation," in *Proceedings of the IEEE/RSJ International Conference on Intelligent Robots and Systems (IROS)*. IEEE, 2011, pp. 4893–4898.
- [30] F. Giovacchini, F. Vannetti, M. Fantozzi, M. Cempini, M. Cortese, A. Parri, T. Yan, D. Lefeber, and N. Vitiello, "A light-weight active orthosis for hip movement assistance," *Robotics and Autonomous Systems*, 2014.
- [31] K. A. Witte, J. Zhang, R. W. Jackson, and S. H. Collins, "Design of two lightweight, high-bandwidth torque-controlled ankle exoskeletons," in *Proceedings of the IEEE International Conference on Robotics and Automation (ICRA)*, Seattle, WA, 2015.
- [32] G. A. Pratt and M. M. Williamson, "Series elastic actuators," in *Proceedings of the IEEE/RSJ International Conference on Intelligent Robots and Systems (IROS)*, vol. 1. IEEE, 1995, pp. 399–406.
- [33] M. Zinn, O. Khatib, B. Roth, and J. K. Salisbury, "Playing it safe [human-friendly robots]," *IEEE Robotics & Automation Magazine*, vol. 11, no. 2, pp. 12–21, 2004.
- [34] D. W. Robinson, J. E. Pratt, D. J. Paluska, and G. A. Pratt, "Series elastic actuator development for a biomimetic walking robot," in *Advanced Intelligent Mechatronics, 1999. Proceedings. 1999 IEEE/ASME International Conference on*. IEEE, 1999, pp. 561–568.
- [35] G. A. Pratt, P. Willisson, C. Bolton, and A. Hofman, "Late motor processing in low-impedance robots: impedance control of series-elastic actuators," in *Proceedings of the American Control Conference*, vol. 4. IEEE, 2004, pp. 3245–3251.
- [36] G. Wyeth, "Control issues for velocity sourced series elastic actuators," in *Proceedings of the Australasian Conference on Robotics and Automation 2006*. Australian Robotics and Automation Association Inc, 2006.
- [37] A. Schiele, P. Letier, R. van der Linde, and F. Van der Helm, "Bowden cable actuator for force-feedback exoskeletons," in *Proceedings of the IEEE/RSJ International Conference on Intelligent Robots and Systems (IROS)*. IEEE, 2006, pp. 3599–3604.
- [38] D. Hobbelen, T. de Boer, and M. Wisse, "System overview of bipedal robots flame and tulip: Tailor-made for limit cycle walking," in *Proceedings of the IEEE/RSJ International Conference on Intelligent Robots and Systems (IROS)*. IEEE, 2008, pp. 2486–2491.
- [39] L. M. Mooney, E. J. Rouse, and H. M. Herr, "Autonomous exoskeleton reduces metabolic cost of human walking during load carriage," *Journal of NeuroEngineering and Rehabilitation*, vol. 11, no. 80, pp. 0003–11, 2014.
- [40] J. F. Veneman, R. Ekkelenkamp, R. Kruidhof, F. C. van der Helm, and H. van der Kooij, "A series elastic-and bowden-cable-based actuation system for use as torque actuator in exoskeleton-type robots," *International Journal of Robotics Research*, vol. 25, no. 3, pp. 261–281, 2006.
- [41] J. M. Caputo and S. H. Collins, "Prosthetic ankle push-off work reduces metabolic rate but not collision work in non-amputee walking," *Scientific reports*, vol. 4, 2014.
- [42] K. Kong, J. Bae, and M. Tomizuka, "Control of rotary series elastic actuator for ideal force-mode actuation in human-robot interaction applications," *IEEE Transactions on Mechatronics*, vol. 14, no. 1, pp. 105–118, 2009.
- [43] D. Zanotto, T. Lenzi, P. Stegall, and S. K. Agrawal, "Improving transparency of powered exoskeletons using force/torque sensors on the supporting cuffs," in *Proceedings of the IEEE International Conference on Rehabilitation Robotics (ICORR)*. IEEE, 2013, pp. 1–6.
- [44] W. van Dijk, H. Van Der Kooij, B. Koopman, and E. van Asseldonk, "Improving the transparency of a rehabilitation robot by exploiting the cyclic behaviour of walking," in *Proceedings of the IEEE International Conference on Rehabilitation Robotics (ICORR)*. IEEE, 2013, pp. 1–8.
- [45] S. H. Collins and R. W. Jackson, "Inducing self-selected human engagement in robotic locomotion training," in *Proceedings of the IEEE International Conference on Rehabilitation Robotics (ICORR)*. IEEE, 2013, pp. 1–6.
- [46] D. A. Winter, *The biomechanics and motor control of human gait: normal, elderly and pathological*, 2nd ed. Waterloo: University of Waterloo Press, 1991.
- [47] D. P. Ferris, K. E. Gordon, G. S. Sawicki, and A. Peethambaran, "An improved powered ankle-foot orthosis using proportional myoelectric control," *Gait & posture*, vol. 23, no. 4, pp. 425–428, 2006.
- [48] J. H. Kim and J. H. Oh, "Walking control of the humanoid platform khr-1 based on torque feedback control," in *Proceedings of the IEEE International Conference on Robotics and Automation (ICRA)*, 2004, pp. 623–628.
- [49] S. H. Collins, M. B. Wiggin, and G. S. Sawicki, "Reducing the energy cost of human walking using an unpowered exoskeleton," *Nature*, vol. 522, pp. 212–215, 2015.
- [50] H. Vallery, R. Ekkelenkamp, H. Van Der Kooij, and M. Buss, "Passive and accurate torque control of series elastic actuators," in *Proceedings of the IEEE/RSJ International Conference on Intelligent Robots and Systems (IROS)*. IEEE, 2007, pp. 3534–3538.
- [51] T. Lenzi, N. Vitiello, S. M. M. De Rossi, S. Roccella, F. Vecchi, and M. C. Carrozza, "Neuroexos: a variable impedance powered elbow exoskeleton," in *Proceedings of the IEEE International Conference on Robotics and Automation (ICRA)*. IEEE, 2011, pp. 1419–1426.
- [52] N. Paine, S. Oh, and L. Sentis, "Design and control considerations for high-performance series elastic actuators," *Mechatronics, IEEE/ASME Transactions on*, vol. 19, no. 3, pp. 1080–1091, 2014.
- [53] T. Nef, M. Mihelj, G. Kiefer, C. Perndl, R. Muller, and R. Riener, "ARMin-exoskeleton for arm therapy in stroke patients," in *Proceedings of the IEEE International Conference on Rehabilitation Robotics (ICORR)*. IEEE, 2007, pp. 68–74.
- [54] A. Gupta, M. K. O'Malley, V. Patoglu, and C. Burgar, "Design, control and performance of RiceWrist: A force feedback wrist exoskeleton for rehabilitation and training," *International Journal of Robotics Research*, vol. 27, no. 2, pp. 233–251, 2008.
- [55] R. J. Farris, H. Quintero, M. Goldfarb *et al.*, "Preliminary evaluation of a powered lower limb orthosis to aid walking in paraplegic individuals," *Neural Systems and Rehabilitation Engineering, IEEE Transactions on*, vol. 19, no. 6, pp. 652–659, 2011.
- [56] S. Arimoto and M. Takegaki, "A new feedback method for dynamic control of manipulators," *J. Dyn. Systems, Measurement Control*, vol. 102, pp. 119–125, 1981.
- [57] R. Kelly, "Regulation of manipulators in generic task space: An energy shaping plus damping injection approach," *Robotics and Automation, IEEE Transactions on*, vol. 15, no. 2, pp. 381–386, 1999.
- [58] L. L. Cai, A. J. Fong, C. K. Otsoshi, Y. Liang, J. W. Burdick, R. R. Roy, and V. R. Edgerton, "Implications of assist-as-needed robotic step training after a complete spinal cord injury on intrinsic strategies of motor learning," *The Journal of neuroscience*, vol. 26, no. 41, pp. 10564–10568, 2006.
- [59] S. K. Banala, S. H. Kim, S. K. Agrawal, and J. P. Scholz, "Robot assisted gait training with active leg exoskeleton (ALEX)," *IEEE Transactions on Neural Systems and Rehabilitation Engineering*, vol. 17, no. 1, pp. 2–8, 2009.
- [60] J. Zhang, C. C. Cheah, and S. H. Collins, "Stable human-robot interaction control for upper-limb rehabilitation robotics," in *Proceedings of the IEEE International Conference on Robotics and Automation (ICRA)*. IEEE, 2013, pp. 2201–2206.
- [61] C. Fleischer, C. Reinicke, and G. Hommel, "Predicting the intended motion with EMG signals for an exoskeleton orthosis controller," in

- Proceedings of the IEEE/RSJ International Conference on Intelligent Robots and Systems (IROS)*. IEEE, 2005, pp. 2029–2034.
- [62] J. Zhang and C. C. Cheah, “Passivity and stability of human–robot interaction control for upper-limb rehabilitation robots,” *IEEE Transactions on Robotics*, vol. 31, pp. 233–245, 2015.
- [63] R. Ortega and M. W. Spong, “Adaptive motion control of rigid robots: A tutorial,” *Automatica*, vol. 25, no. 6, pp. 877–888, 1989.
- [64] A. Calanca and P. Fiorini, “Human-adaptive control of series elastic actuators,” *Robotica*, vol. 32, no. 08, pp. 1301–1316, 2014.
- [65] J. Bae and M. Tomizuka, “A gait rehabilitation strategy inspired by an iterative learning algorithm,” *Mechatronics*, vol. 22, no. 2, pp. 213–221, 2012.
- [66] P. Malcolm, R. E. Quesada, J. M. Caputo, and S. H. Collins, “The influence of push-off timing in a robotic ankle-foot prostheses on the energetics and mechanics of walking,” *Journal of NeuroEngineering and Rehabilitation*, vol. 12, no. 21, pp. 1–14, 2015.
- [67] K. B. Fite and M. Goldfarb, “Design and energetic characterization of a proportional-injector monopropellant-powered actuator,” *IEEE Transactions on Mechatronics*, vol. 11, no. 2, pp. 196–204, 2006.
- [68] J. K. Hitt, T. G. Sugar, M. Holgate, and R. Bellman, “An active foot-ankle prosthesis with biomechanical energy regeneration,” *Journal of Medical Devices*, vol. 4, no. 1, p. 011003, 2010.
- [69] J. Rosen, M. Brand, M. B. Fuchs, and M. Arcan, “A myosignal-based powered exoskeleton system,” *Systems, Man and Cybernetics, Part A: Systems and Humans*, *IEEE Transactions on*, vol. 31, no. 3, pp. 210–222, 2001.
- [70] E. Cavallaro, J. Rosen, J. C. Perry, S. Burns, and B. Hannaford, “Hill-based model as a myoprocessor for a neural controlled powered exoskeleton arm –parameters optimization,” in *Proceedings of the IEEE International Conference on Robotics and Automation (ICRA)*, Barcelona, Spain, Apr. 2005.
- [71] J. C. Perry, J. Rosen, and S. Burns, “Upper-limb powered exoskeleton design,” *IEEE Transactions on Mechatronics*, vol. 12, no. 4, pp. 408–417, 2007.
- [72] M. F. Eilenberg, H. Geyer, and H. Herr, “Control of a powered ankle–foot prosthesis based on a neuromuscular model,” *IEEE Transactions on Neural Systems and Rehabilitation Engineering*, vol. 18, no. 2, pp. 164–173, 2010.
- [73] H. Geyer and H. Herr, “A muscle-reflex model that encodes principles of legged mechanics produces human walking dynamics and muscle activities,” *IEEE Transactions on Neural Systems and Rehabilitation Engineering*, vol. 18, no. 3, pp. 263–273, 2010.
- [74] A. H. Shultz, J. E. Mitchell, D. Truex, B. E. Lawson, E. Ledoux, and M. Goldfarb, “A walking controller for a powered ankle prosthesis,” in *Engineering in Medicine and Biology Society (EMBC), 2014 36th Annual International Conference of the IEEE*. IEEE, 2014, pp. 6203–6206.
- [75] T. W. Dorn, J. M. Wang, J. L. Hicks, and S. L. Delp, “Predictive simulation generates human adaptations during loaded and inclined walking,” *PloS one*, vol. 10, no. 4, 2015.
- [76] N. Van der Noot, A. J. Ijspeert, and R. Ronsse, “Biped gait controller for large speed variations, combining reflexes and a central pattern generator in a neuromuscular model,” in *Proceedings of the IEEE International Conference on Robotics and Automation (ICRA)*. IEEE, 2015, pp. 6267–6274.
- [77] J. Markowitz, P. Krishnaswamy, M. F. Eilenberg, K. Endo, C. Barnhart, and H. Herr, “Speed adaptation in a powered transtibial prosthesis controlled with a neuromuscular model,” *Philosophical Transactions of the Royal Society B: Biological Sciences*, vol. 366, no. 1570, pp. 1621–1631, 2011.
- [78] C. Loconsole, S. Dettori, A. Frisoli, C. A. Avizzano, and M. Bergamasco, “An emg-based approach for on-line predicted torque control in robotic-assisted rehabilitation,” in *Haptics Symposium (HAPTICS), 2014 IEEE*. IEEE, 2014, pp. 181–186.
- [79] S. Huang, J. P. Wensman, and D. P. Ferris, “An experimental powered lower limb prosthesis using proportional myoelectric control,” *Journal of Medical Devices*, vol. 8, no. 2, p. 024501, 2014.
- [80] K. Z. Takahashi, M. D. Lewek, and G. S. Sawicki, “A neuromechanics-based powered ankle exoskeleton to assist walking post-stroke: a feasibility study,” *Journal of neuroengineering and rehabilitation*, vol. 12, no. 1, p. 23, 2015.
- [81] A. B. Zoss, H. Kazerooni, and A. Chu, “Biomechanical design of the berkeley lower extremity exoskeleton (bleex),” *IEEE Transactions on Mechatronics*, vol. 11, no. 2, pp. 128–138, 2006.
- [82] S. Wang, C. Meijneke, and H. Van Der Kooij, “Modeling, design, and optimization of mindwalker series elastic joint,” in *Proceedings of the IEEE International Conference on Rehabilitation Robotics (ICORR)*. IEEE, 2013, pp. 1–8.
- [83] J. S. Sulzer, R. Roiz, M. Peshkin, J. L. Patton *et al.*, “A highly backdrivable, lightweight knee actuator for investigating gait in stroke,” *IEEE Transactions on Robotics*, vol. 25, no. 3, pp. 539–548, 2009.
- [84] T. Kobayashi, Y. Akazawa, H. Naito, M. Tanaka, S. W. Hutchins *et al.*, “Design of an automated device to measure sagittal plane stiffness of an articulated ankle-foot orthosis,” *Prosthetics and Orthotics International*, vol. 34, no. 4, pp. 439–448, 2010.
- [85] D. Accoto, G. Carpino, F. Sergi, N. L. Tagliamonte, L. Zollo, and E. Guglielmelli, “Design and characterization of a novel high-power series elastic actuator for a lower limb robotic orthosis,” *International Journal of Advanced Robotic Systems*, vol. 10, p. 359, 2013.
- [86] J. Gordon and C. Ghez, “Trajectory control in targeted force impulses,” *Experimental brain research*, vol. 67, no. 2, pp. 253–269, 1987.
- [87] A. Klimchik, A. Pashkevich, D. Chablat, and G. Hovland, “Compensation of compliance errors in parallel manipulators composed of non-perfect kinematic chains,” in *Latest Advances in Robot Kinematics*. Springer, 2012, pp. 51–58.
- [88] J.-J. E. Slotine and W. Li, “On the adaptive control of robot manipulators,” *The international journal of robotics research*, vol. 6, no. 3, pp. 49–59, 1987.
- [89] J.-J. E. Slotine, W. Li *et al.*, *Applied nonlinear control*. Prentice-hall Englewood Cliffs, NJ, 1991, vol. 199, no. 1.
- [90] S. Arimoto, S. Kawamura, and F. Miyazaki, “Bettering operation of robots by learning,” *Journal of Robotic systems*, vol. 1, no. 2, pp. 123–140, 1984.
- [91] G. Heinzinger, D. Fenwick, B. Paden, and F. Miyazaki, “Stability of learning control with disturbances and uncertain initial conditions,” *IEEE Transactions on Automatic Control*, vol. 37, no. 1, pp. 110–114, 1992.
- [92] J. Van de Wijdeven, T. Donkers, and O. Bosgra, “Iterative learning control for uncertain systems: robust monotonic convergence analysis,” *Automatica*, vol. 45, no. 10, pp. 2383–2391, 2009.
- [93] E. Schuitema, M. Wisse, T. Ramakers, and P. Jonker, “The design of LEO: a 2D bipedal walking robot for online autonomous reinforcement learning,” in *Proceedings of the IEEE/RSJ International Conference on Intelligent Robots and Systems (IROS)*. IEEE, 2010, pp. 3238–3243.
- [94] S. M. Cain, K. E. Gordon, and D. P. Ferris, “Locomotor adaptation to a powered ankle-foot orthosis depends on control method,” *Journal of NeuroEngineering and Rehabilitation*, vol. 4, 2007.
- [95] S. K. Au, P. Dilworth, and H. Herr, “An ankle-foot emulation system for the study of human walking biomechanics,” in *Proceedings of the*

- IEEE International Conference on Robotics and Automation (ICRA)*. IEEE, 2006, pp. 2939–2945.
- [96] S. Song, J. Kim, and K. Yamane, “Development of a bipedal robot that walks like an animation character,” in *Proceedings of the IEEE International Conference on Robotics and Automation (ICRA)*, 2015, pp. 3596–3602.
- [97] J. G. Ziegler and N. B. Nichols, “Optimum settings for automatic controllers,” *trans. ASME*, vol. 64, no. 11, 1942.
- [98] S. W. Sung and I.-B. Lee, “Limitations and countermeasures of pid controllers,” *Industrial & engineering chemistry research*, vol. 35, no. 8, pp. 2596–2610, 1996.
- [99] C. A. Desoer and M. Vidyasagar, *Feedback systems: input-output properties*. SIAM, 1975, vol. 55.
- [100] S. Arimoto, *Control Theory of Nonlinear Mechanical Systems*. Oxford University Press, Inc., 1996.